ROMP Synthesis of Side-Chain Ferrocene-Containing Polyelectrolyte and Its Redox-Responsive Hydrogels Showing Dramatically Improved Swelling with β-Cyclodextrin

Qiangjun Ling, Fangchen Zhen, Didier Astruc, Haibin Gu

ROMP Synthesis of Side-Chain Ferrocene-Containing Polyelectrolyte and Its Redox-Responsive Hydrogels Showing Dramatically Improved Swelling with β-Cyclodextrin

Qiangjun Ling, Fangchen Zhen, Didier Astruc, Haibin Gu**

Q. Ling, Dr. H. Gu.
Key Laboratory of Leather Chemistry and Engineering of Ministry of Education, National Engineering Research Center of Clean Technology in Leather Industry, Sichuan University, Chengdu 610065, China.
E-mail: guhaibinkong@126.com

F. Zheng,
MaCSE,
Rennes Institute of Chemical Sciences, Bât 10B, UMR CNRS N°6226, University of Rennes 1, Campus de Beaulieu, 263 Avenue du Général Leclerc, 35042 Rennes Cedex, France

Prof. D. Astruc
ISM, UMR CNRS 5255
Univ. Bordeaux, 33405 Talence Cedex, France
E-mail: didier.astruc@u-bordeaux.fr

A new side-chain ferrocene (Fc)-containing polyelectrolyte has been synthesized by controlled ring-opening metathesis polymerization of a water-soluble Fc-containing norbornene-based quaternary ammonium salt, as well as the corresponding covalently cross-linked polyelectrolyte hydrogel. In order to provide Fc-containing supramolecular polyelectrolyte hydrogels whose swelling property are largely improved by host−guest interaction, a covalently cross-linked polyelectrolyte hydrogel was soaked into the β-CD aqueous solution to form β-CD@Fc supramolecular polyelectrolyte hydrogel, or alternatively the quaternary ammonium salt supramolecular monomer was first formed, then copolymerized with a crosslinking agent to fabricate the supramolecular hydrogel with better water absorption ability. All the Fc-containing hydrogels exhibited good redox-responsiveness with swelling−shrinking behaviors by chemically reversibly adjusting the disassembly/assembly of β-CD@Fc inclusion complexes. This is the first example of side-chain Fc-containing polycationic supramolecular hydrogels possessing swelling−shrinking properties based on the splitting/combining of β-CD and Fc units, and potential applications are expected as controlled drug delivery and actuators.

1. Introduction

The past decades witnessed the rapid development of ferrocenyl (Fc)-containing polymers and their functional applications in various fields, [1-3] such as drug delivery, [4,5] magneto-ceramics, [6] electro-chromics, [7] hydrogels, [8-10] biomaterials, [11] sensors, [12,13] catalysis, [14] and stimuli-responsive materials. [15] Especially, the elegant application of ring-opening polymerization (ROP) of strained silicon-bridged [1] ferrocenophane monomers led to a whole chemistry field of poly (ferrocenylsilanes) (PFS)-based main-chain Fc-containing homopolymers and copolymers. [16] Side-chain Fc-containing polymers [17] were also synthesized by various living and controlled polymerization techniques including atom transfer radical polymerization (ATRP), [18] reversible addition fragmentation chain transfer polymerization (RAFT), [19] and ring-opening metathesis polymerization (ROMP). [20,21]

Water-soluble Fc-containing polymers are increasingly required in their application areas including hydrogels, drug delivery, nanomedicine, and bio-sensing. [22,23] Many efforts have been paid to transfer the hydrophobic Fc-containing polymers into water. The co-polymerization of hydrophilic and hydrophobic ferrocenyl monomers is the most frequently investigated method to yield water-soluble Fc-containing polymers. For example, Natalello [24] and co-workers developed main-chain Fc-containing PFS-based amphiphilic and water-soluble block copolymers through epoxide termination of PFS block as a macroinitiator for the subsequent living anionic ROP of ethylene oxide monomer. Liu et al. [25] described the synthesis of side-chain Fc-containing amphiphilic dendronized random copolymer using direct ROMP of a hydrophilic macromonomer containing nine branches of triethylene glycol and a hydrophobic macromonomer bearing nine Fc units. Alkan et al. [26] reported the synthesis of amphiphilic side-chain Fc-containing block copolymers via the anionic ROP of ferrocenyl glycidyl ether using hydrophilic poly (ethylene glycol) (PEG) monomethyl ether as the macroinitiator and their application as redox-active micellar nano-carriers and smart surfactants.

Water-soluble Fc-containing polycations and polyanions have also been synthesized by post-polymerization side-chain modification of PFS. [27-30] These polymers are valuable, because they combine the unique properties of PFS with the processability of polyelectrolytes, and they have been successfully applied to fabricate various functional materials including layer-by-layer films, [31-33] microgels [34] and hydrogels. [35-37] For instance, Hempenius et al.[30] described typical synthesis routes of cationic and anionic PFS-based polyelectrolytes. Poly (ferrocenyl(3-iodopropyl) methylsilane) (PFS-I) was firstly obtained via halogen exchange reaction, then transferred to the corresponding polycation containing iodide counterions by its quaternization reaction with *N*,*N*-dimethylethylamine. Its chloride analogue with higher water-solubility was further obtained through exchange reaction of iodide counterions with chloride counterions. The anionic polyelectrolyte was also prepared by nucleophilic reaction of PFS-I with α-lithioisobutylmethanesulfonate, followed by exchange of the tetrabutylammonium counterions with sodium ions. Although many examples of the main-chain Fc-containing polyelectrolytes have already been reported in the literature, the side-chain ones are seldom described. [38]

Covalently cross-linked and Fc-containing hydrogels have recently attracted intense attention because of their excellent redox-responsiveness to external chemical or electrochemical stimuli. [8-10] It is essential and crucial for Fc-containing hydrogels to absorb and keep water, especially towards smart biological applications such as sensing, surface modification and actuators, because this property is closely related to the swelling and shrinking behavior of hydrogels when exposed to outside stimuli. However, the water absorption property of Fc-containing hydrogels reported in the literature is still not satisfactory owing to the strongly hydrophobic nature of the Fc unit. Up to now, the fabrication of Fc-containing hydrogel exhibiting a swelling−shrinking behaviour at the macroscopic scale is still a great challenge.

Herein, we report a new side-chain Fc-containing polyelectrolyte synthesized by controlled ROMP of a water-soluble Fc-containing norbornene-based quaternary ammonium salt and the corresponding covalently cross-linked polyelectrolyte hydrogel fabricated by copolymerizing

this salt with a water-soluble norbornene crosslinking agent (**Scheme 1**). The intense 1:1 complexing ability of Fc unit with β-cyclodextrin (β-CD) prompted us to further develop a new type of side-chain Fc-containing supramolecular polyelectrolyte hydrogels whose swelling property would be strongly improved by host−guest interaction. For this goal, we designed two strategies (**Scheme 1**). In the first route, the prepared covalently cross-linked polyelectrolyte hydrogel containing pendant Fc groups was soaked into the β-CD aqueous solution, and the supramolecular hydrogel with well-swollen performance was obtained. This property is due to the formation of pendant β-CD@Fc inclusion complexes and the resulting transformation of hydrophobic Fc units into hydrophilic moieties. In the second route, the quaternary ammonium salt supramolecular monomer was first formed and then copolymerized with the crosslinking agent to fabricate the supramolecular hydrogel with a better water absorption ability. Both supramolecular hydrogels exhibited good redox-responsiveness with swelling−shrinking behaviors by chemically reversibly adjusting the disassembly/assembly of β-CD@Fc inclusion complexes. To our knowledge, this is the first example of side-chain Fc-containing polycationic hydrogels possessing such swelling−shrinking properties based on the splitting/combination of β-CD and Fc units, and these smart hydrogels are expected to find potential applications in sensing, surface modification and actuation.

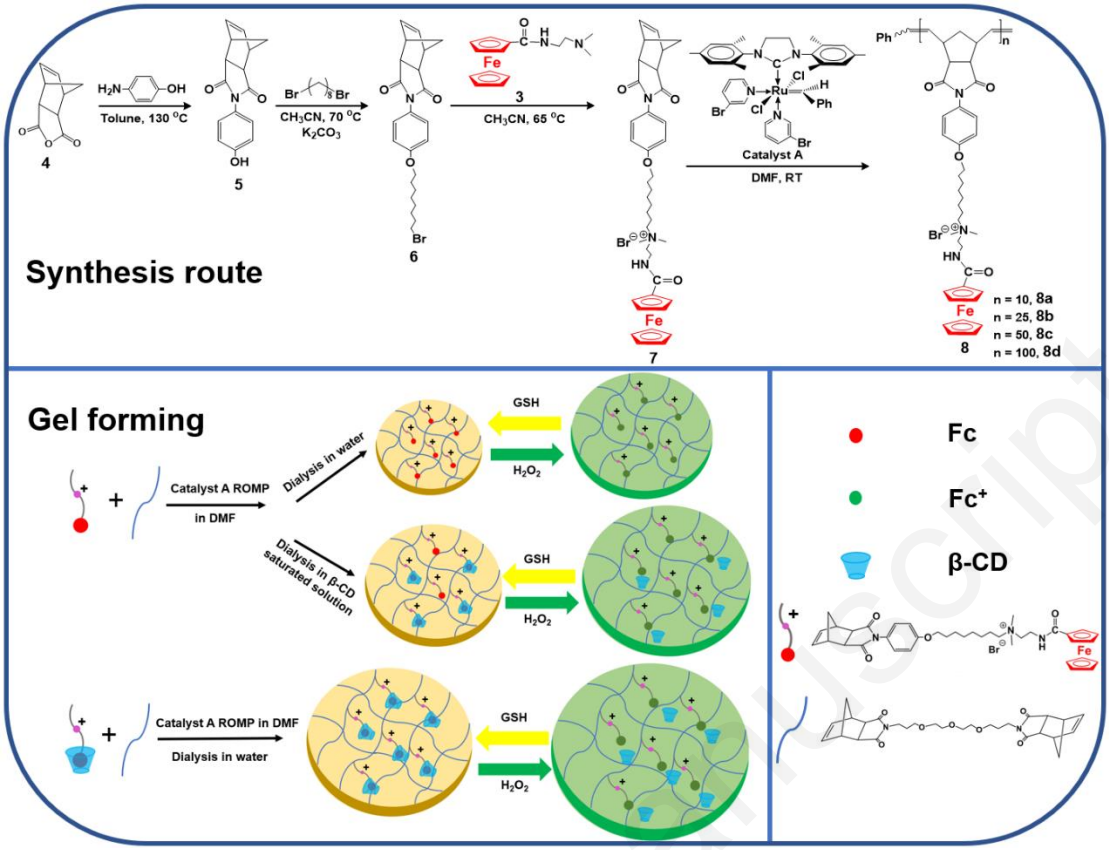

Scheme 1 Synthesis route to side-chain Fc-containing polyelectrolyte and its hydrogels.

2. Results and discussion

2.1. Synthesis and structure of monomer 7 and homopolymer 8

Scheme 1 provides the synthesis route of quaternary ammonium salt monomer **7**. The compound **3** was synthesized by the amidation reaction of ferrocene-carboxylic acid with *N*,*N*-dimethyl-ethylenediamine, while the reaction of cis-5-norbornene-exo-2,3-dicarboxylic anhydride 4 and *p*-aminophenol led to the formation of compound **5** that was then transferred into the key intermediate **6** via treatment with 1,8-dibromooctane. Finally, the targeted monomer **7** was obtained through the quaternary ammonium salt reaction between the reactive bromide group of compound **6** and the amine group of compound **3**. The successful preparation and structures of the quaternary ammonium salt monomer **7** and related intermediates were confirmed by ^{1}H NMR, ^{13}C NMR, MS, IR and UV-vis. spectroscopy, and the details are found in the supplementary information (SI).

The monomer **7** was obtained as an orange powder with hygroscopic property, and exhibited good solubility in water. It can be also dissolved in many polar and nonpolar organic solvents including dichloromethane (CH_2Cl_2), chloroform ($CHCl_3$), tetrahydrofuran (THF), methanol, ethanol, benzene, toluene, ethyl acetate, dimethylformamide (DMF) and dimethyl-sulfoxide (DMSO). It shows insolubility in petroleum ether and diethyl ether.

Using the third-generation Grubbs metathesis catalyst (catalyst A), the ROMP reaction of monomer **7** was carried out at RT (room temperature, 25 °C or so) in DMF to obtain homopolymer **8**. Four feed molar ratios (monomer 7: catalyst A), namely 10: 1, 25: 1, 50: 1 and 100: 1, were adopted to synthesize homopolymers **8** with the desired polymerization degrees of 10, 25, 50 and 100, respectively. The polymerization kinetics of monomer **7** was monitored by using in situ ^{1}H NMR spectroscopy. Concretely, after 5, 15, 30, 60, 120 and 180 min of stirring, respectively, 0.1 mL of reaction mixture was taken out using a syringe, quenched by adding 0.1 mL of EVE, and dried under reduced pressure. Then, the ^{1}H NMR spectrum of the dried reaction mixture was determined using $(CD_3)_2SO$ as the solvent. When the peak at 6.36 ppm disappeared completely, the polymerization of monomer **7** was deemed to be accomplished with the conversion ratio of 100%. As shown in **Figure. S21**, after 30 min of stirring, there is no peak at 6.36 ppm corresponding to the olefinic protons (CH=CH) of monomer 7, and two broad peaks at 5.72 and 5.51 ppm, assigned to the olefinic protons of polynorbornene, were observed. These results demonstrate that all the polymerizations for the synthesis of homopolymers **8a-d** are achieved in 30 min. The successful preparation and structures of homopolymers **8a-d** were also confirmed by ^{1}H NMR, ^{13}C NMR, IR and UV-vis spectroscopy, and the details could be found in supplementary information (SI).

The polymerization degrees of homopolymers **8a-8d** were calculated by using ^{1}H NMR end-group analysis.[41] The calculations were conducted by comparing the intensities of the signals of the five protons of the end-phenyl group with those of the characteristic protons of homopolymers **8** (See details in SI). The obtained polymerization degrees are 10 ± 1 for **8a**

(**Table S3**) 25 ± 2 for **8b** (**Table S4**), 50 ± 3 for **8c** (**Table S5**) and 83 ± 6 for **8d** (**Table S6**), respectively. For the homopolymers **8a-8c**, the calculated values show the high consistency with the theoretical polymerization degrees resulting from the added feed molar ratios of monomer **7** and catalyst A. For homopolymer **8d**, the obtained polymerization degree of 83 ± 6 is also close to the theoretical value of 100. Overall, these results indicate the controlled characteristics for the ROMP reaction of cationic monomer **7**, and namely, the well-defined polyelectrolyte **8** was synthesized by controlling the feed molar ratio between monomer **7** and catalyst A.

All the homopolymers **8a-8d** were also obtained as orange powders and showed different solubility in different solvents. Homopolymers **8a-8d** exhibited good solubility in DMF and DMSO, and insolubility in petroleum ether and diethyl ether. In other organic solvents (e.g. CH_2Cl_2, $CHCl_3$, THF, methanol, toluene) and water, homopolymer **8** possessed decreased solubility along with the increase of molecular weight. For example, like monomer **7**, homopolymer **8a** is easily soluble in water, but when the polymerization degree is increased to 100, the corresponding homopolymer **8d** is only partially soluble in water.

Homopolymer **8** exhibited reversible chemical redox property during an oxidation-reduction cycle. As shown in **Figure. S25**, the addition of $FeCl_3$ as an oxidizing agent led to the color change from the original orange to green, which is attributed to the iron-centered monoelectronic oxidation ($Fe^{II} \rightarrow Fe^{III}$) of the Fc units. [42-44] This transformation was confirmed by the UV-vis. spectrum in which the original λ_{max} peak at 436 nm disappeared and a new λ_{max} peak at 633 nm appeared. After that, the addition of sodium ascorbate as a reducing agent resulted in color change from green to orange, accompanied by the re-appearance of the λ_{max} peak at 436 nm and the disappearance of the λ_{max} peak at 633 nm. These results indicate that the side-chain Fc units in homopolymer **8** were totally reduced into Fc moieties.

The cyclic voltammograms (CVs) of the polymers recorded in DMF using NBu_4PF_6 (2 M) as supporting electrolyte are classic for ferrocene-containing polymers (see SI), showing a single

wave at 0.7 V vs. SCE that appears chemically reversible and electrochemically quasi-reversible with Ep = 200 mV at a scan rate of 2V/s. Thus, slow heterogeneous electron transfer between the ferrocenyl redox centers and the glassy carbon working electrode is observed due to the polymer bulk that inhibits fast structural rearrangement in the course of heterogeneous electron transfer.[45,46] This situation contrasts with that of Fc-terminated dendrimers for which the CVs of the Fc group appears Nerstian, signifying fast electron transfers from the Fc redox sites to the electrode due to inter-site hoping and/or fast dendrimer rotation within the electrochemical time scale.[47,48] Overall, this shows the remarkable specificity of each type of Fc-containing macromolecule.

2.2. Covalent cross-linking hydrogel CC-Fc-HG

Figure. 1A shows the SEM image of lyophilized **CC-Fc-HG**. The honeycomb-like porous microstructure was observed with the pore size of 120 ± 30 µm. Also, the EDS analysis indicates the existence of the Fe and Br elements, which is attributed to the successful polymerization of monomer 7 during the fabrication of **CC-Fc-HG**.

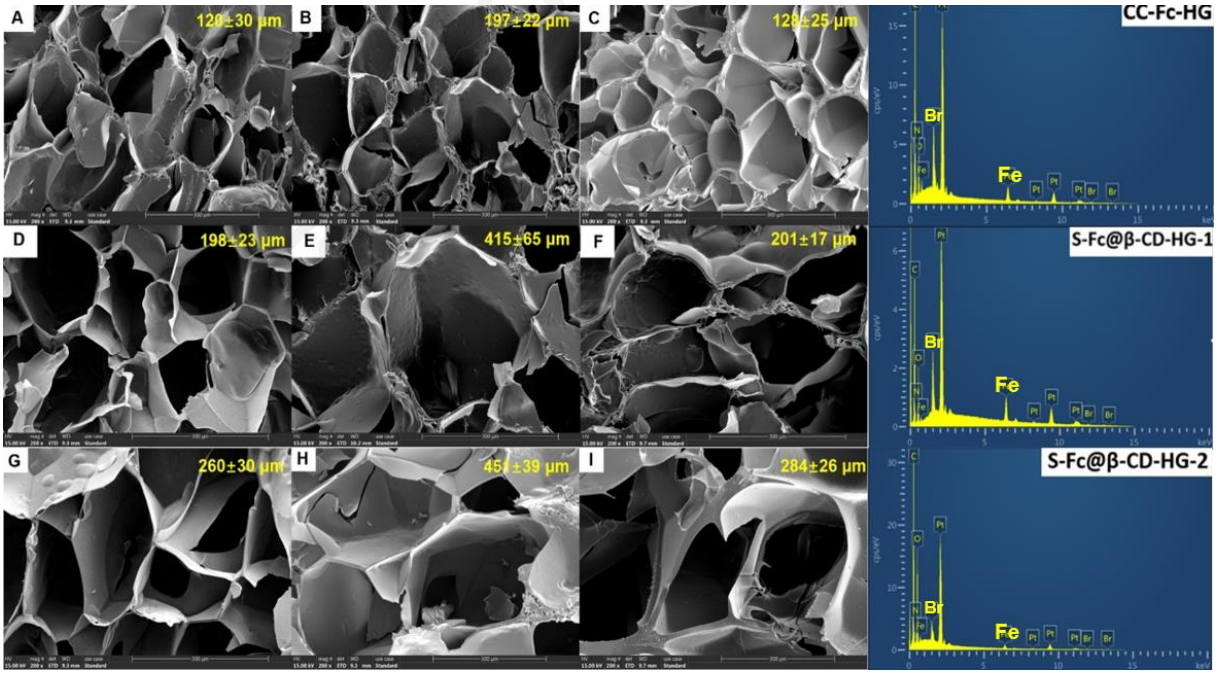

Figure. 1 SEM images and EDS results of **CC-Fc-HG** (A-C), **S-Fc@β-CD-HG-1** (D-F) and **S-Fc@β-CD-HG-2** (G-I) during an oxidation-reduction cycle. A, D and G are the original; B, E and H are the oxidized; C, F and I are the reduced.

The water-absorbing property of **CC-Fc-HG** was determined by using the gravimetric method. Specially, the freeze-dried hydrogel **CC-Fc-HG** was immersed into deionized water at RT for 120 h to reach the adsorption equilibrium. At different intervals, the weight of **CC-Fc-HG** was recorded, and its water absorption rate (WAR) was calculated. The water absorption curve was then drawn by using the soaking time as the x-coordinate and WAR as the y-coordinate. As shown in **Figure. 2A**, **CC-Fc-HG** exhibits slow water-absorbing kinetics, and the equilibrium WAR reaches 130%. In other words, the freeze-dried **CC-Fc-HG** absorbs 1.3 times its weight in water. This water-absorbing property is attributed to the side-chain hydrophilic quaternary ammonium salt groups of the polyelectrolyte 8 framework.

The thermal stability of **CC-Fc-HG** was determined by DSC and TG. The DSC curve (**Figure. 3**) provides the glass-transition temperature (T_g) of 57 °C, while the TG/DTG curves (**Figure. 4A**) indicates three weight-loss stages. The first weight-loss stage, that is attributed to the loss of water, is observed at 30-120 °C with the weight-loss ratio of 1%. The second and third weight-loss stages appear at 120-440 °C (peak at 235 °C) and 400-800 °C (peak at 458 °C), and the corresponding weight-loss ratios without water are 53% and 9%. The final residual rate reaches 38% (**Table 1**). The second weight-loss stage resulted from the decomposition of the organic polynorbornene network, while the third stage was caused by the degradation of the Fc units.

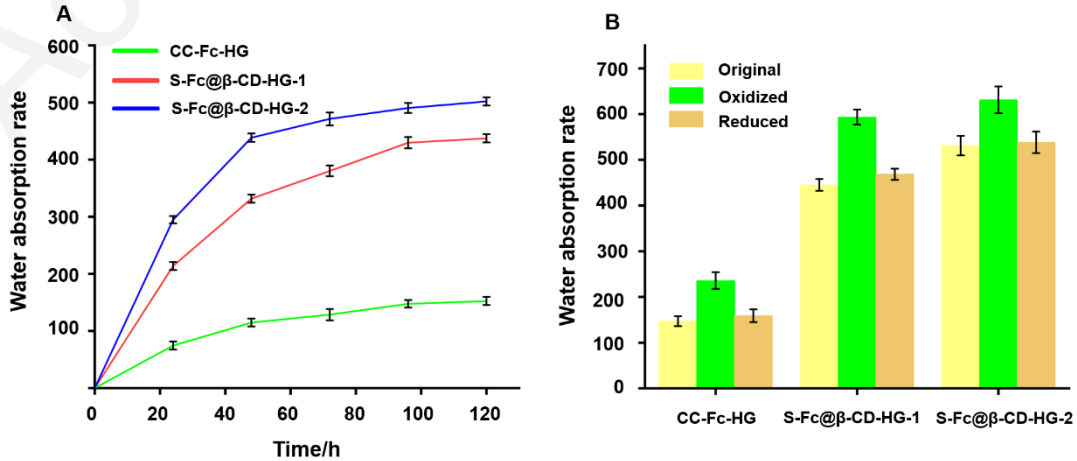

Figure. 2 Water absorption curves (A) of **CC-Fc-HG**, **S-Fc@β-CD-HG-1** and **S-Fc@β-CD-HG-2** and their equilibrium water absorption rates (B) during an oxidation-reduction cycle.

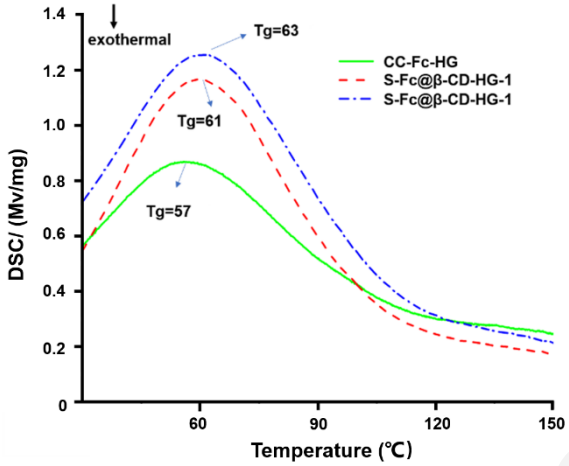

Figure. 3 DSC curves of **Fc-HG, Fc@β-CD-HG-1 and Fc@β-CD-HG-2.**

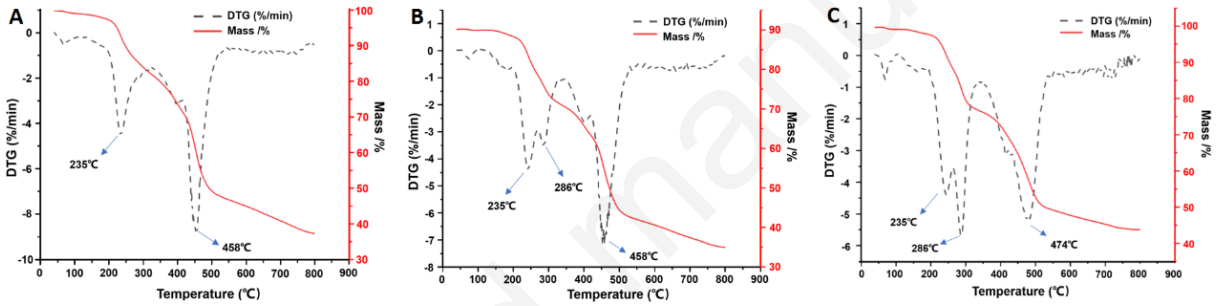

Figure. 4 TG and DTG curves of **CC-Fc-HG** (A), **S-Fc@β-CD-HG-1** (B) and **S-Fc@β-CD-HG-2** (C).

Table 1 Weight-Loss Ratio (%) of Hydrogels from TG Curves

Hydrogel	The first stage (30-120 °C)	The second stage (120-440 °C)	The third stage (440-800 °C)	Residual rate
CC-Fc-HG	1	52/53[a]	9/9[a]	37/38[a]
S-Fc@β-CD-HG-1	3	46/48[a]	7/7[a]	44/45[a]
S-Fc@β-CD-HG-2	1	48/49[a]	6/6[a]	45/45[a]

[a]Weight-loss ratio calculated when the water content is totally removed.

Figure. 5 shows the rheological analysis results of **CC-Fc-HG**. As shown **Figure. 5A**, the storage modulus G' and loss modulus G'' were recorded when the strain was changed in the range of 0.1-1000% and the angular frequency was fixed at 1 rad/s. When the stain was less than 10%, the value of G' was larger than that of G'', indicating the elasticity of the hydrogel network **CC-Fc-HG**. When the stain was further increased, both G' and G'' rapidly decreased,

and G' intersected with G" at the stain of 110%, which is explained by the collapse of the hydrogel network. [49] G' and G'' were also recorded when the angular frequency was changed in the range of 0.1-100 rad/s, and the stain was fixed at 1%. As depicted in **Figure. 5B**, the value of G' is much greater than that of G'', and both G' and G" have no change in the whole frequency change scope, indicating that they were relatively independent of the frequency and thus of the stable structure of the hydrogel network.

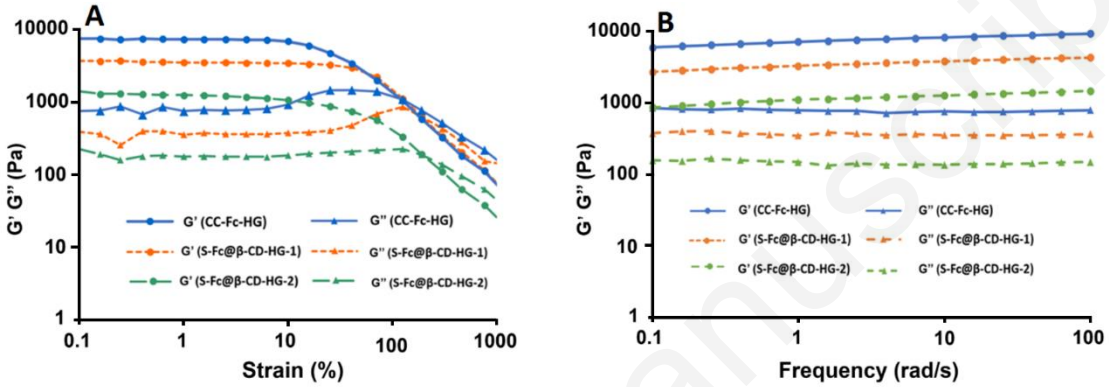

Figure. 5 (A) Linear viscoelastic zone (strain: 0.1-1000%, frequency: 1rad/s; temperature: 25°C) and (B) frequency sweep test (0.1-100 rad/s) at fixed strain of 1% of **CC-Fc-HG**, **S-Fc@β-CD-HG-1** and **S-Fc@β-CD-HG-2**.

The redox-responsive swelling behavior of **CC-Fc-HG** was determined during an oxidation-reduction cycle. A hydrogel disc of **CC-Fc-HG** with a diameter of 20 mm was immersed into the aqueous solution of hydrogen peroxide (H_2O_2, 35%). After 1 h of soaking at RT, color change from the original orange to green was observed, and the diameter of the disc increased to 23 mm (**Figure. 6A**). The swelling of the hydrogel disc was also confirmed by the significant increase of the equilibrium WAR from the original 130% to 240% (**Figure. 2B**). Furthermore, the SEM image of the oxidized hydrogel disc was also recorded and, as expected, increased pore size of 197 ± 22 μm was observed (**Figure. 1B**). The oxidized hydrogel disc was then immersed into the aqueous solution of glutathione (GSH) for 1 h, and the color change was observed from green to orange, accompanied by the recovery of the diameter of the disc from 23 mm to 20 mm (**Figure. 6A**). This recovery was also confirmed by the SEM image (**Figure.**

1C) indicating the reduced pore size of 128 ± 25 μm as well as the decreased equilibrium WAR of 140% **(Figure. 2B**). The neutral Fc group is hydrophobic, whereas the cationic Fc^+ unit is hydrophilic. Thus, the positively charged pendant Fc^+ units resulted from the Fc oxidation by H_2O_2 and the positively charged quaternary ammonium salt structures led to the more positively polymer hydrogel network. It promoted the macroscopic swelling of the hydrogel **CC-Fc-HG** whose previous expansion was caused by the electrostatic repulsion among side chains. On the contrary, when the cationic Fc^+ unit was reduced to neutral Fc by GSH, macroscopic shrinking of **CC-Fc-HG** was observed because of the decreased positive charge in the side chains.

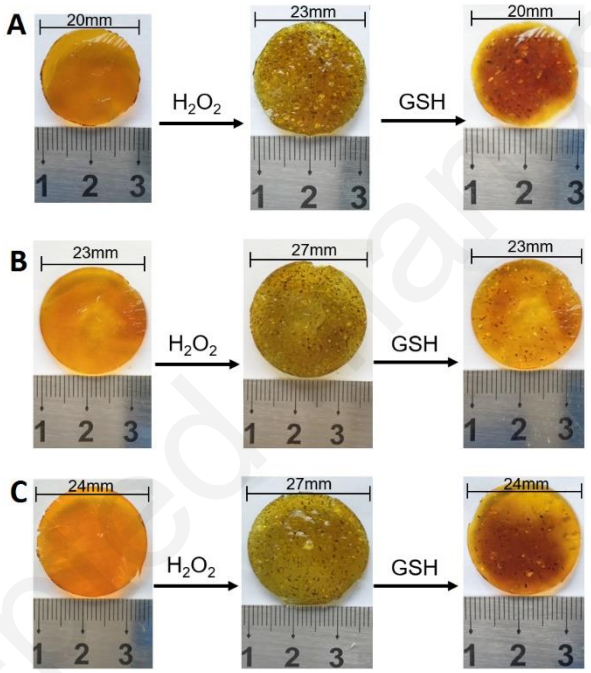

Figure. 6 Photographs of **CC-Fc-HG** (A), **S-Fc@β-CD-HG-1** (B) and **S-Fc@β-CD-HG-2** (C) during an oxidation-reduction cycle.

2.3. Supramolecular hydrogel S-Fc@β-CD-HG-1

The host-guest 1:1 complexation of β-CD with Fc has been confirmed in many reports, [50,51] and this interaction transfers the hydrophobic Fc group into the hydrophilic β-CD/Fc inclusion complex. Considering this point, the supramolecular hydrogel **S-Fc@β-CD-HG-1** was further fabricated through dialysis treatment of the organo-gel **CC-Fc-HG** against the saturated aqueous solution of β-CD. As shown in **Figure. S29**, compared to the hydrogel **CC-Fc-HG**

that was obtained by dialysis against deionized water, the hydrogel **S-Fc@β-CD-HG-1** exhibited increased bulk indicating its improved water absorption by the hydrogel network. Specially, the diameter of 15 mm for the **S-Fc@β-CD-HG-1** hydrogel column is much larger than that of 12 mm for the **CC-Fc-HG** one.

Figure. 1D provides the SEM image of the freeze-dried **S-Fc@β-CD-HG-1**. The honeycomb-like porous microstructure was also observed with an increased pore size of 198 ± 23 μm, which is explained by the improved hydrophilicity of the pendant β-CD/Fc inclusion complexes formed during the dialysis. Moreover, the EDS analysis confirms the existence of the Fe and Br elements.

The water absorption curve of the freeze-dried **S-Fc@β-CD-HG-1** was also recorded by using the gravimetric method, and compared with that of **CC-Fc-HG**. As shown in **Figure. 2A**, **S-Fc@β-CD-HG-1** exhibits significantly much higher water-absorbing ability, and the equilibrium WAR achieves 400%. Namely, the freeze-dried **S-Fc@β-CD-HG-1** absorbs 4 times its weight in water. This increased water-absorbing property is attributed to the transformation of the side-chain hydrophobic Fc units into the hydrophilic β-CD/Fc inclusion complexes.

DSC and TG were also emplyed to characterize the thermal stability of **S-Fc@β-CD-HG-1**. As depicted in **Figure. 3**, the T_g value of 61 °C, provided by the DSC curve of **S-Fc@β-CD-HG-1**, is slightly higher than that (57 °C) of **CC-Fc-HG**, which is probably explained by the increased intermolecular interaction owing to the formation of β-CD/Fc inclusion complexes. Similarly, there are also three weight-loss stages in the TG/DTG curves of **S-Fc@β-CD-HG-1** (**Figure. 4B**). The first weight-loss stage, attributed to the loss of water, is observed at 30-120 °C with the weight-loss ratio of 3%. The second weight-loss stage appears at 120-440 °C with 48% of weight-loss ratio without water, but there are two peaks. The first peak is found at 235 °C, which is due to the decomposition of organic polynorbornene network; the second peak is observed at 286 °C, which probably results from the thermal decomposition of the β-CD

structure. Like in the case of **CC-Fc-HG**, the third weight-loss stage of 7% is found at 400-800 °C, and the peak is observed at 458 °C, which is caused by the degradation of the Fc units. The rheological tests were also conducted to determine the mechanical property of **S-Fc@β-CD-HG-1**. As shown in **Figure. 5A**, like in the case of **CC-Fc-HG**, G' and G'' of **S-Fc@β-CD-HG-1** exhibit similar change tendency when the strain was changed in the range of 0.1-1000%. Concretely, when the stain was less than 50%, the G' value was larger than that of G'', indicating the elastic network of hydrogel **S-Fc@β-CD-HG-1**. When the stain was further increased, both G' and G'' rapidly decreased, and G' intersected with G" at the stain of 200%, which is explained by the collapse of the hydrogel network.[50] These values of both G' and G'' are smaller than those of **CC-Fc-HG**, indicating the decreased mechanic property of **S-Fc@β-CD-HG-1**. Furthermore, G' and G'' were also recorded when the angular frequency was changed in the range of 0.1-100 rad/s and the stain was fixed at 1%. As depicted in **Figure. 5B**, the value of G' is much greater than that of G'', and both G' and G" did not change in the whole frequency change scope, indicating that they were relatively independent of the frequency and thus the stable structure of the hydrogel network. Similarly, frequency sweep test results of **S-Fc@β-CD-HG-1** are smaller than that of **CC-Fc-HG**.

The redox-sensitive swelling behavior of **S-Fc@β-CD-HG-1** was also investigated during an oxidation-reduction cycle. A hydrogel disc of **S-Fc@β-CD-HG-1** with a diameter of 24 mm was soaked in the aqueous solution of H_2O_2 (35%). After 1 h of soaking at RT, the clear color change from the original orange to green was observed, and the diameter of the disc was increased to 27 mm (**Figure. 6B**). The swelling of the hydrogel disc was also confirmed by the significant increase of the equilibrium WAR from the original 450% to 600% (**Figure. 2B**). Furthermore, the SEM image of the oxidized hydrogel disc was also recorded, and, as expected, increased pore size of 415 ± 65 μm was observed (**Figure. 1E**). The oxidized hydrogel disc was then immersed into the aqueous solution of GSH for 1 h, and the color change was observed from green to orange, accompanied by the recovery of the diameter of the disc from 27 mm to

24 mm. This recovery was also confirmed by the SEM image (**Figure. 1F**), indicating the reduced pore size of 201 ± 17 μm, as well as the decreased equilibrium WAR of 450% (**Figure. 2B**). Like in the case of **CC-Fc-HG**, the swelling-shrinking behavior of **S-Fc@β-CD-HG-1** is also explained by the oxidation-reduction cycle of its side-chain Fc units. The oxidation by H_2O_2 led to the transformation of hydrophobic neutral Fc groups into hydrophilic cationic Fc^+ units, and thus the macroscopic swelling of hydrogel **S-Fc@β-CD-HG-1**. The subsequent reduction by GSH resulted in the recovery of hydrophobic neutral Fc groups from hydrophilic cationic Fc^+ units, and thus the macroscopic shrinking of **S-Fc@β-CD-HG-1**.

2.4. Supramolecular hydrogel S-Fc@β-CD-HG-2

The direct polymerization method was also used to prepare the Fc-containing supramolecular hydrogel **S-Fc@β-CD-HG-2** using a supramolecular monomer formed by the host-guest interaction between β-CD and monomer **7**. Using the enhancement of nuclear Overhauser effect when protons are close to each other, [52] we confirmed the formation of this supramolecular monomer through the 2D NOESY NMR spectrum method. **Figure. 7** shows the 2D NOESY NMR spectrum of equimolar monomer **7** and β-CD in D_2O. There are intersection points at 3.60-3.84 ppm and 4.20-4.30 ppm, and the former corresponds to the internal H3 and H5 protons of β-CD cavity, while the latter originates from the free Cp protons of the Fc unit. The appearance of these intersection points confirms the formation of supramolecular monomer via the host-guest complexation between the β-CD ring and the Fc unit in monomer **7**.

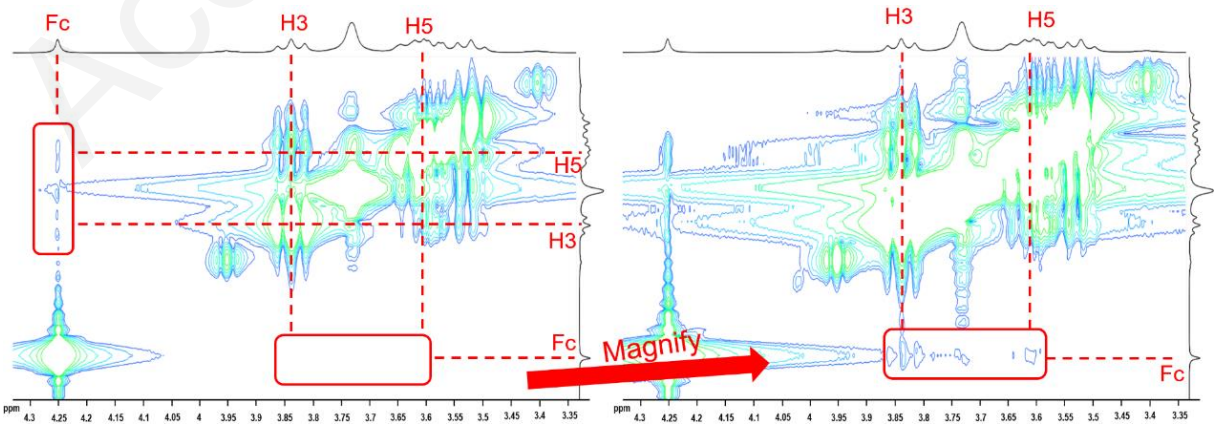

Figure. 7 2D NOESY NMR spectrum in D_2O of the mixture of monomer **7** and β-CD at the equimolar ratio.

Figure. 1G shows the SEM image of lyophilized **S-Fc@β-CD-HG-2**. Like in the case of **CC-Fc-HG** and **S-Fc@β-CD-HG-1**, the microstructure of **S-Fc@β-CD-HG-2** exhibits the honeycomb-like porous characteristic, but it has the largest pore size of 260 ± 30 μm. Also, the EDS analysis indicates the existence of the Fe and Br elements, which reflects the successful polymerization of the Fc-containing supramolecular monomer during the fabrication of **S-Fc@β-CD-HG-2**.

The greatest water-absorbing ability of **S-Fc@β-CD-HG-2** was also confirmed by its water absorption curve shown in **Figure. 2A**. Compared to **S-Fc@β-CD-HG-1**, **S-Fc@β-CD-HG-2** exhibits a much higher water-absorbing ability, and the equilibrium WAR reaches 500%. Namely, the freeze-dried **S-Fc@β-CD-HG-2** absorbs 5 times its weight in water. **S-Fc@β-CD-HG-1** and **S-Fc@β-CD-HG-2** have similar composition and structure, but the latter has greater water-absorbing ability than the former, which was attributed to the more hydrophilic β-CD/Fc inclusion complexes and free β-CD fixed in the hydrogel network of the latter.

The thermal stability of **S-Fc@β-CD-HG-2** was also investigated using both DSC and TG techniques. As depicted in **Figure. 3**, the T_g value of 63 °C, provided by the DSC curve of **S-Fc@β-CD-HG-2**, is slightly higher than that (61 °C) of **S-Fc@β-CD-HG-1**, which is probably explained by the increased intermolecular interaction owing to the much larger amount of β-CD/Fc inclusion complexes and free β-CD fixed in the hydrogel network of **S-Fc@β-CD-HG-2**. Compared to **S-Fc@β-CD-HG-1**, **S-Fc@β-CD-HG-2** exhibits similar TG/DTG curves, and there are also three weight-loss stages (**Figure. 4C**). The first weight-loss stage, attributed to the loss of water, is observed at 30-120 °C with a weight-loss ratio of 1%. The second weight-loss stage appears at 120-440 °C with 49% of weight-loss ratio without water, and there are two peaks, too. The first peak is found at 235 °C, due to the decomposition of organic polynorbornene network; the second peak is observed at 286 °C, probably resulting from thermal decomposition of the β-CD structure. In the second stage, **S-Fc@β-CD-HG-2** exhibits

higher weight-loss ratio than **S-Fc@β-CD-HG-1**, attributed to the more β-CD structures in **S-Fc@β-CD-HG-2**. In the third weight-loss stage of 400-800 ℃, **S-Fc@β-CD-HG-2** exhibits 6% of weight-loss ratio without water, and the peak was observed at 474 ℃, caused by the degradation of the Fc units.

The mechanical property of **S-Fc@β-CD-HG-1** was also evaluated through the rheological tests. As shown in **Figure. 5A**, like in the case of **S-Fc@β-CD-HG-1**, G' and G'' of **S-Fc@β-CD-HG-2** exhibit similar change tendency when the strain was changed in the range of 0.1-1000%. Concretely, when the stain was less than 50%, the value of G' was larger than that of G'', indicating the elasticity of network of hydrogel **S-Fc@β-CD-HG-2**. When the stain was further increased, both G' and G'' rapidly decreased, and G' intersected with G" at the stain of 200%, which is explained by the collapse of the hydrogel network.[50] These values of both G' and G'' of **S-Fc@β-CD-HG-2** are smaller than those of **S-Fc@β-CD-HG-1**, indicating the decreased mechanic property of **S-Fc@β-CD-HG-2**. Furthermore, G' and G'' were also recorded when the angular frequency was changed in the range of 0.1-100 rad/s, and the stain was fixed at 1%. As depicted in **Figure. 5B**, the value of G' is much larger than that of G'', and both G' and G" do not change in the whole frequency change scope, indicating their relatively independency of the frequency and thus the stability the hydrogel network structure. Similarly, frequency sweep test results of **S-Fc@β-CD-HG-2** are smaller than that of **S-Fc@β-CD-HG-1**, indicating its worse mechanical property than that of the latter.

The redox-responsive swelling-shrinking behavior of **S-Fc@β-CD-HG-2** was also investigated during an oxidation-reduction cycle. A hydrogel disc of **S-Fc@β-CD-HG-2** with a diameter of 26 mm was immersed into the aqueous solution of H_2O_2 (35%). After 1 h of soaking at RT, the color change from the original orange to green was observed, and the diameter of the disc was increased to 28 mm (**Figure. 6C**). The swelling of the hydrogel disc was also confirmed by the significant increase of the equilibrium WAR from the original 500% to 620% (**Figure. 2B**). The SEM image of the oxidized hydrogel disc was also recorded and, as expected, an increased

pore size of 451 ± 39 μm was observed (**Figure. 1H**). The oxidized hydrogel disc was then immersed into the aqueous solution of GSH for 1 h, and the color change from green to orange was observed and accompanied by a diameter change of the disc from 28 mm to 25 mm (**Figure 6C**). This change was also confirmed by the SEM image (**Figure. 1I**), indicating the reduced pore size of 284 ± 26 μm, as well as the decreased equilibrium WAR of 500% (**Figure. 2B**). Like in the case of **CC-Fc-HG** and **S-Fc@β-CD-HG-1**, the swelling-shrinking behavior of **S-Fc@β-CD-HG-2** is also explained by the oxidation-reduction cycle of its side-chain Fc units. The oxidation by H_2O_2 led to the transformation of hydrophobic neutral Fc groups into hydrophilic cationic Fc^+ units and thus to the macroscopic swelling of hydrogel **S-Fc@β-CD-HG-2**. The subsequent reduction by GSH resulted in the recovery of the hydrophobic neutral Fc groups from the hydrophilic cationic Fc^+ units and thus in the macroscopic shrinking of **S-Fc@β-CD-HG-2**.

Conclusions

In summary, a new type of side-chain Fc-containing water-soluble polyelectrolyte with various polymerization degrees was successfully and controllably synthesized via ROMP of a Fc-containing norbornene-based quaternary ammonium salt with the aid of the third-generation Grubbs metathesis catalyst. Using the ROMP method, the corresponding covalently cross-linked polyelectrolyte hydrogel was further successfully fabricated. Both designed strategies were successfully carried out to prepare the supramolecular polyelectrolyte hydrogel. In the soaking method, the pendant hydrophobic Fc units in the network of covalently cross-linked polyelectrolyte hydrogel was encapsulated by hydrophilic β-CD rings, leading to the formation of supramolecular hydrogel with well-swollen performance. Furthermore, the quaternary ammonium salt supramolecular monomer was formed owing to the 1:1 host-guest complexation between β-CD and Fc and copolymerized with the crosslinking agent to fabricate the supramolecular hydrogel with better water absorption ability. The prepared covalently cross-

linked and supramolecular hydrogels possessed good redox-responsiveness with swelling−shrinking behavior by chemical reversibly adjusting the disassembly/assembly of β-CD@Fc inclusion complexes. These smart Fc-containing polyelectrolyte hydrogels are expected to find potential applications as controlled drug delivery and actuators.

Conflicts of interest

There are no conflicts to declare.

Acknowledgements

Helpful discussion with Dr Philippe Hapiot (Rennes) and financial support by the National Natural Science Foundation of China (No. 21978180), the Science & Technology Department of Sichuan Province (No. 2018HH0038), the Universities of Bordeaux and Rennes 1 and the Centre National de la Recherche Scientifique (CNRS) are gratefully acknowledged.

Supplementary information

Syntheses spectra, cyclic voltammograms, calculation of polymer degrees for homopolymers **8a-d**, redox properties of monomer **7** and homopolymer **8** and solubility of monomer **7** and homopolymers **8**.

Key words

ROMP; Polyelectrolyte; Ferrocene; β-Cyclodextrin; Host-guest interaction; Supramolecular hydrogel; Redox-responsiveness.

References

[1] G. R. Whittell, M. D. Hager, U. S. Schubert, I. Manners, *Nat. Mater.*, **2011**, *10*, 176-188.

[2] M. Gallei and C. Ruettiger, Chem.-Eur. J., **2018**, *24*, 10006−10021.

[3] D. Astruc, *Eur. J. Inorg. Chem.*, **2017**, 6−29.

[4] H. B. Gu, S. D. Mu, G. R. Qiu, X. Liu, L. Zhang, Y. F. Yuan, D. Astruc, *Coord. Chem. Rev.*, **2018**, *364*, 51−85.

[5] G. I. Dzhardimalieva, L. N. Rabinskiy, K. A. Kydralieva, I. E. Uflyand, *RSC Adv.*, **2019**, *9*, 37009−37051.

[6] H. K. Li, W. W. Chi, Y. J. Liu, W. Yuan, Y. W. Li, Y. F. Li, B. Z. Tang, *Macromol. Rapid Commun.*, **2017**, *38*, 1700075.

[7] H. B. Gu, R. Ciganda, P. Castel, S. Moya, R. Hernandez, J. Ruiz, D. Astruc, *Angew. Chem., Int. Ed.*, **2018**, *57*, 2204–2208.

[8] J. L. Wu, L. Wang, H. J. Yu, Zain-ul-Abdin, R. U. Khan, M. Haroon, *J. Organomet. Chem.*, **2017**, *828*, 38−51.

[9] H. Li, P. Yang, P. Pageni, C. B. Tang, *Macromol. Rapid Commun.*, **2017**, *38*, 1700109.

[10] X. Liu, L. Zhao, F. F. Liu, D. Astruc, H. B. Gu, *Coord. Chem. Rev.*, **2020**, *419*, 213406.

[11] A. S. Abd-El-Aziz, C, Agatemor, N. Etkin, *Biomaterials*, **2017**, *118*, 27−50.

[12] R. L. Sun, L. Wang, H. J. Yu, Zain-ul-Abdin, Y. S. Chen, J. Huang, R. B. Tong, *Organometallics*, **2014**, *33*, 4560−4573.

[13] M. Saleem, H.J. Yu, L. Wang, Zain-ul-Abdin, H. Khalid, M. Akram, N. M. Abbasi, J. Huang, *Anal. Chim. Acta.*, **2015**, *876*, 9−25.

[14] F. F. Liu, X. Liu, D. Astruc, H. B. Gu, *J. Colloid Interface Sci.*, **2019**, *533*, 161-170.

[15] K. Y. Zhang, S. J. Liu, Q. Zhao, W. Huang, *Coord. Chem. Rev.*, **2016**, *319*, 180−195.

[16] R. L. N. Hailes, A. M. Oliver, J. Gwyther, G. R. Whittell, I. Manners, *Chem. Soc. Rev.*, **2016**, *45*, 5358−5407.

[17] C. G. Hardy, J. Y. Zhang, Y. Yan, L. X. Ren, C. B. Tang, *Prog. Polym. Sci.*, **2014**, *39*, 1742–1796.

[18] W. H. Qian, H. Y. Zhang, T. Song, M. Ye, C. Feng, G. L. Lu, X. Y. Huang, *Eur. Polym. J.*, **2019**, *119*, 8−13.

[19] P. Yang, P. Pageni, M. P. Kabir, T. Y. Zhu, C. B. Tang, *ACS Macro Lett.*, **2016**, *5*, 1293–1300.

[20] X. Liu, A. Rapakousiou, C. Deraedt, R. Ciganda, Y. L. Wang, J. Ruiz, H. B. Gu, D. Astruc, *Chem. Commun.*, **2020**, *56*, 11374–11385.

[21] X. Liu, F. F. Liu, W. T. Liu, H. B. Gu, *Polym. Rev.*, **2020**, DOI:10.1080/15583724.2020.1723022.

[22] A. Alkan, F. R. Wurm, *Macromol. Rapid Commun.*, **2016**, *37*, 1482−1493.

[23] T. Y. Zhu, Y. Sha, J. Yan, P. Pageni, M. A. Rahman, Y. Yan, C. B. Tang, *Nat. Commun.*, **2018**, *9*, 4329.

[24] A. Natalello, A. Alkan, A. Friedel, I. Lieberwirth, H. Frey, F. R. Wurm, *ACS Macro Lett.*, **2013**, *2*, 313–316.

[25] X. Liu, F. F. Liu, Y. L. Wang, H. B. Gu, *React. Funct. Polym.*, **2019**, *143*, 104325.

[26] A. Alkan, S. Wald, B. Louage, B. G. De Geest, K. Landfester, F. R. Wurm, *Langmuir*, **2017**, *33*, 272−279.

[27] K. N. Power-Billard, I. Manners, *Macromolecules*, **2000**, *33*, 26−31.

[28] M. A. Hempenius, N. S. Robins, R. G. H. Lammertink, G. J. Vancso, *Macromol. Rapid Commun.*, **2001**, *22*, 30−33.

[29] M. A. Hempenius and G. J. Vancso, *Macromolecules*, **2002**, *35*, 2445−2447.

[30] M. A. Hempenius, F. F. Brito, G. J. Vancso, *Macromolecules*, **2003**, *36*, 6683−6688.

[31] M. A. Hempenius, M. Peter, N. S. Robins, E. S. Kooij, G. J. Vancso, *Langmuir*, **2002**, *18*, 7629−7634.

[32] E. S. Kooij, Y. J. Ma, M. A. Hempenius, G. J. Vancso, B. Poelsema, *Langmuir*, **2010**, *26*, 14177−14181.

[33] X. L. Feng, H. R. Wu, X. F. Sui, M. A. Hempenius, G. J. Vancso, *Eur. Polym. J.*, **2015**, *72*, 535−542.

[34] X. F. Sui, L. L. Shui, J. Cui, Y. B. Xie, J. Song, A. van den Berg, M. A. Hempenius, G. J. Vancso, *Chem. Commun.*, **2014**, *50*, 3058−3060.

[35] B. Zoetebier, M. A. Hempenius, G. J. Vancso, *Chem. Commun.*, **2015**, *51*, 636−639.

[36] X. L. Feng, K. H. Zhang, P. Chen, X. F. Sui, M. A. Hempenius, B. Liedberg, G. J. Vancso, *Macromol. Rapid Commun.*, **2016**, *37*, 1939−1944.

[37] K. H. Zhang, X. L. Feng, C. N. Ye, M. A. Hempenius, G. J. Vancso, *J. Am. Chem. Soc.*, **2017**, *139*, 10029−10035.

[38] K. J. Watson, S. T. Nguyen, C. A. Mirkin, *J. Organomet. Chem.*, **2000**, *606*, 79−83.

[39] H. B. Gu, A. Rapakousiou, P. Castel, N. Guidolin, N. Pinaud, J. Ruiz, D. Astruc, *Organometallics,* **2014**, *33,* 4323-4335.

[40] J. A. Love, J. P. Morgan, T. M. Trnka, R. H. Grubbs, *Angew. Chem. Int. Ed.*, **2002**, *41*, 4035-4037.

[41] B. Song, G. R. Qiu, W. X. Wang, H. B. Gu, *Des. Monomers Polym.*, **2020**, *23*, 141−154.

[42] A. M. Spring, F. Qiu, J. X. Hong, A. Bannaron, S. Yokoyama, *Polymer.*, **2017**, *119*, 13-27.

[43] X. Liu, W. Lin, D. Astruc, H. B. Gu, *Prog. Polym. Sci.*, **2019**, *96*, 43-105.

[44] D. Astruc, *J. Leather. Sci. Eng.*, **2020**, *2*, 13.

[45] N. G. Connelly, W. E. Geiger, *Chem. Rev.*, **1996**, *96*, 877-910.

[46] D. Astruc, *Electron Transfer and Radical Processes in Transition Metal Chemistry*. VCH, New York, **1995**, Chap. 2.

[47] C. Ornelas, J. Ruiz, C. Belin, D. Astruc *J. Am. Chem. Soc.*, **2009**, *131*, 590-601.

[48] D. Astruc, *Nat. Chem.*, **2012**, *4*, 255-267.

[49] M. L. Song, H. Y. Yu, J. Y. Zhu, Z. F. Ouyang, S. Y. H. Abdalkarim, K. C. Tam, Y. Z. Li, *Chem. Eng. J.*, **2020**, *398*, 125547.

[50] A. Harada, Y. Takashima, Nakahata, *Acc. Chem. Res.*, **2014**, *47*, 2128−2140.

[51] Q. D. Hu, G. P. Tang, P. K. Chu, *Acc. Chem. Res.*, **2014**, *47*, 2017−2025.

[52] S. D. Mu, Q. J. Ling, X. Liu, J. Ruiz, D. Astruc, H. B. Gu, *J. Inorg. Biochem.*, **2019**, *193*, 31−41.

Supplementary Information

ROMP Synthesis of Side-Chain Ferrocene-Containing Polyelectrolyte and Its Redox-Responsive Hydrogels Showing Dramatically Improved Swelling with β-Cyclodextrin

Qiangjun Ling, Fangchen Zhen, Didier Astruc, Haibin Gu**

Q.Ling, Dr. H.Gu.
Key Laboratory of Leather Chemistry and Engineering of Ministry of Education, National Engineering Research Center of Clean Technology in Leather Industry, Sichuan University, Chengdu 610065, China.
E-mail: guhaibinkong@126.com

F.Zheng,
MaCSE,
Rennes Institute of Chemical Sciences, Bât 10B, UMR CNRS N°6226, University of Rennes 1, Campus de Beaulieu, 263 Avenue du Général Leclerc, 35042 Rennes Cedex, France

Prof. D. Astruc
ISM
Université de Bordeaux, UMR CNRS 5255, 33405 Talence Cedex, France
E-mail: didier.astruc@u-bordeaux.fr

Content

Instruments 25
1. Synthesis 25
1.1. Synthesis of 3 25
1.2. Synthesis of 5 28
1.3. Synthesis of 6 29
1.4. Synthesis of monomer 7 31
1.5. Synthesis of homopolymer 8 33
2. Cyclic voltammograms 37
3. Kinetic study and end-group analysis 39
3.1. Kinetic study 39
3.2. Calculation of polymer degrees for homopolymers 8a-d by ^{1}H NMR end-group analysis 40
4. Solubility of monomer 7 and homopolymers 8. 44
5. Redox properties of monomer 7 and homopolymer 8 44
6. Synthesis of crosslinking agent 10 45
7. Preparation and characterization of Fc-containing hydrogels 47
Covalent cross-linking Fc-containing hydrogel (CC-Fc-HG): 47
Supramolecular β-CD/Fc host-guest interaction based hydrogel S-Fc@β-CD-HG-1: 47
Supramolecular β-CD/Fc host-guest interaction based hydrogel S-Fc@β-CD-HG-2: 48
7.1. Determination of water-absorbing property 49
7.2. Redox-responsibility of hydrogels 49

Instruments

^{1}H NMR (400 MHz) and ^{13}C NMR (100 MHz) spectra were recorded at 25 °C using a Bruker AC (400 MHz) spectrometer. All the chemical shifts are reported in parts per million (δ, ppm) with reference to tetramethylsilane (TMS). Mass spectra were recorded using an Applied Biosystems Voyager-DE STR-MALDI-TOF spectrometer. The infrared spectra were recorded on an ATI Mattson Genesis series FT-IR spectrophotometer at the range of 400-4000 cm^{-1}. UV-visible absorption spectra were measured with a Perkin-Elmer Lambda 19 UV-visible spectrometer. Rheological property of hydrogels was determined by Rheometer (Discovery HR-2, TA company, USA). SEM images were recorded on a Scanning electron microscope (Aztec X-Max20, Hitachi). Thermal properties were determined on Differential Scanning Calorimetry Analyzer (DSC 200 PC, Netzsch, Germany) and Thermogravimetric Analyzer (TG 209 F1, Netzsch, Germany).

Materials

Cis-5-norbornene-*exo*-2,3-dicarboxylic anhydride, *p*-aminophenol, 1,8-dibromooctane, ferrocene, *o*-chlorobenzoyl chloride, oxalyl chloride, trimethylamine (Et_3N), *N*,*N*-dimethylethylenediamine, ethyl vinyl ether (EVE), glutathione (GSH), hydrogen peroxide (H_2O_2), β-cyclodextrin (β-CD), and the second generation Grubbs metathesis catalyst were purchased from Energy Chemical (Shanghai, China) and used directly. Ferrocene-carboxylic acid [39] and the third-generation Grubbs metathesis catalyst (catalyst A) [40] were synthesized following the reported procedures. All the other chemicals were from commercial sources and used as received. All the solvents used were dried and freshly distilled.

1. Synthesis

1.1. Synthesis of 3

Ferrocene carboxylic acid (10.0 g, 43.5 mmol, 1 equiv) was dissolved by dichloromethane (CH_2Cl_2, 50 mL) in a 100 mL round-bottomed flask. Oxalyl chloride (55 g, 435 mmol, 10 equiv) was then added dropwise into the above solution at 0 °C under the

stirring condition. The obtained reaction mixture was stirred at 0 °C for 12 h under N_2 atmosphere. Then, CH_2Cl_2 and the excess oxalyl chloride were removed *in vacuo* using a rotary evaporator, and the crude chlorocarbonylferrocene was obtained as reddish solid and used directly in the following reaction. *N*,*N*-Dimethyl-1,2-ethanediamine (4.7 g, 53.3 mmol, 1.2 equiv) and Et_3N (11 g, 109 mmol, 2.5 equiv) were dissolved by CH_2Cl_2 (40 mL) in a round-bottomed flask. The above crude ferrocenyl chloride dissolved in 25 mL of CH_2Cl_2 was then slowly injected at 0 °C into the solution under the stirring condition. After that, the obtained reaction mixture was further stirred at room temperature (RT, 25 °C) for 12 h under N_2 atmosphere. The solvent and excess Et_3N were removed using a rotary evaporator, and the residue was purified by column chromatography with CH_2Cl_2/methanol (100/1, v/v) as the eluent to provide the compound **3** as yellow solid. Yield: 52%. ^{1}H NMR (400 MHz, $CDCl_3$, 25 °C, TMS), δ_{ppm}: 6.43 (s, 1H, NH), 4.64 (d, *J* = 3.9 Hz, 2H, sub. Cp, Cp = η^5-C_5H_5), 4.26 (d, *J* = 3.6 Hz, 2H, sub. Cp), 4.13 (s, 5H, free Cp), 3.47 (q, *J* = 12 Hz, 2H, CONHC***H₂***), 2.53 (t, *J* = 11.9 Hz, 2H, CH_2N), 2.32 (s, 6H, 2 × CH_3). ^{13}C NMR (100 MHz, $(CD_3)_2SO$, 25 °C, TMS), δ_{ppm}: 169.4 (C=ONH), 77.1, 70.4, 69.9, 68.6 (Cp), 58.6 ($NHCH_2$), 45.2 (CH_3), 36.9 (CH_2N). MS (ESI, m/z), calcd. for $C_{15}H_{20}N_2OFe$: 300.00; found: 301.00 $[M+H]^+$. Selected IR (KBr, cm^{-1}): 3292(υ_{NH}), 2927, 2823, 1625 ($\upsilon_{C=O}$), 1543, 1466, 1378, 1306, 1189, 821 (υ_{FeII}).

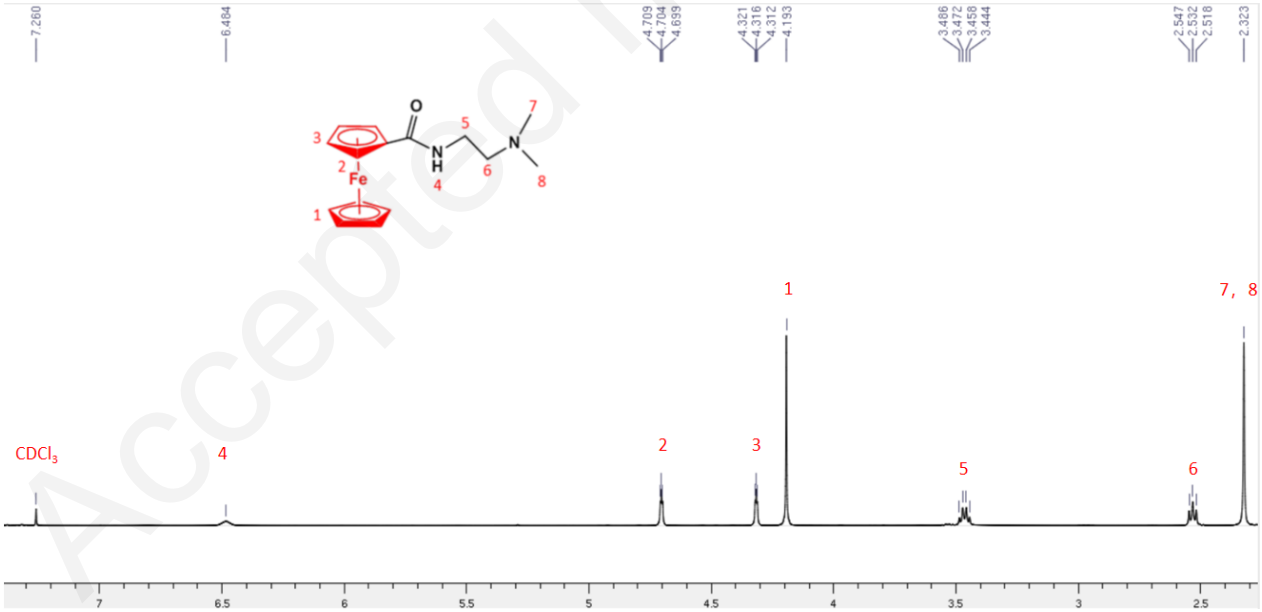

Figure S1 ^{1}H NMR spectrum of **3** in $CDCl_3$.

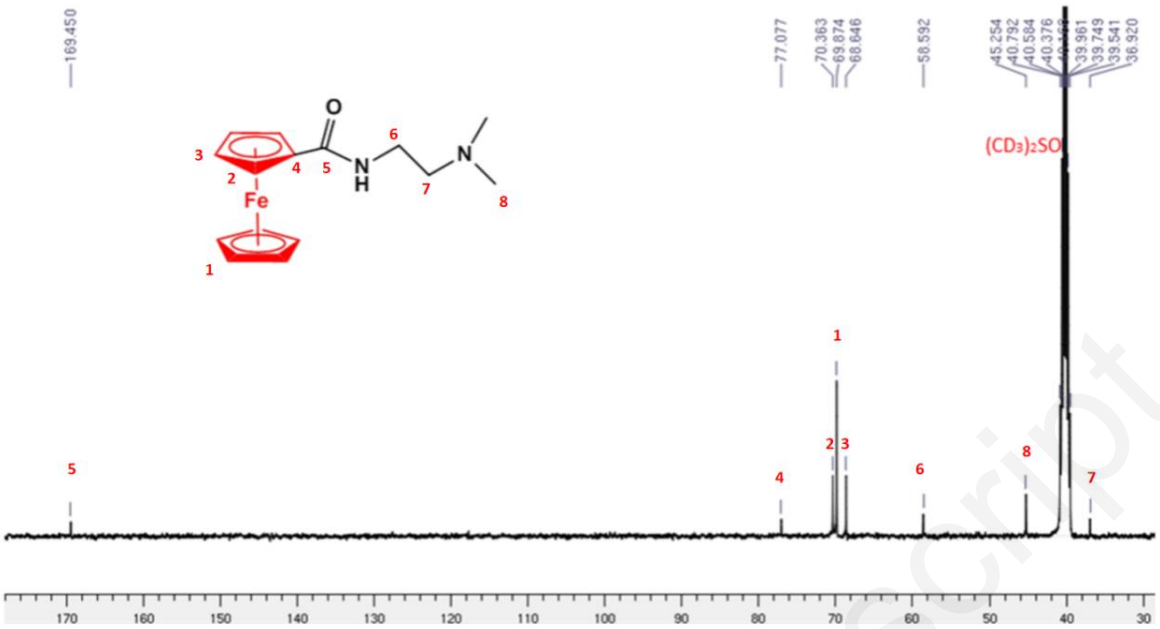

Figure S2 ^{13}C NMR spectrum of **3** in $(CD_3)_2SO$.

Figure S3 Mass spectrum of **3**.

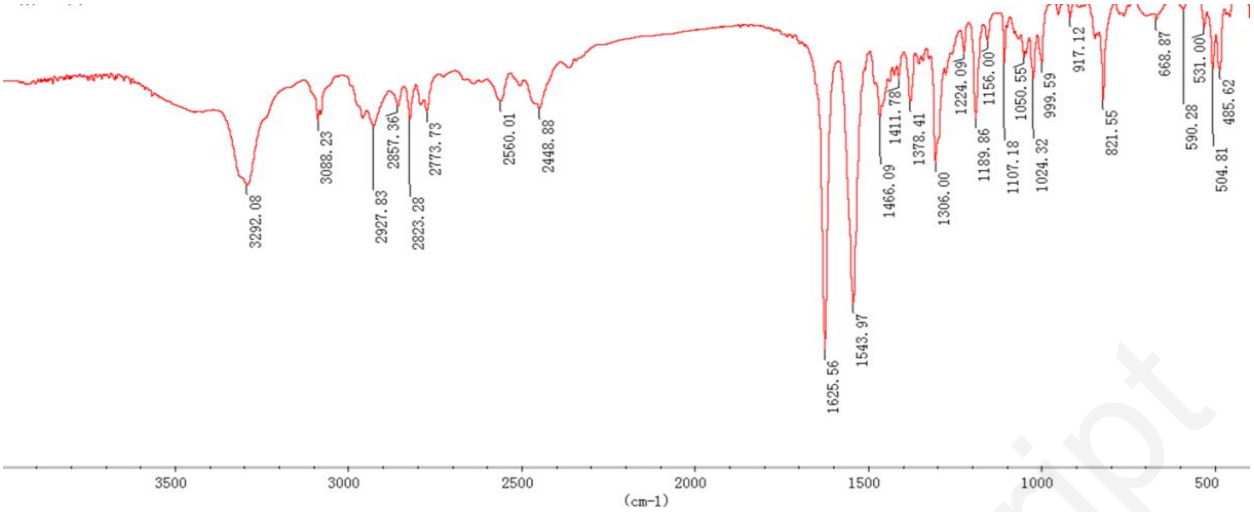

Figure S4 IR spectrum of **3**.

1.2. Synthesis of 5

Cis-5-norbornene-*exo*-2,3-dicarboxylic anhydride (8.0 g, 49 mmol, 1 equiv), Et_3N (4.9 g, 49 mmol, 1 equiv) and *p*-aminophenol (5.3 g, 49mmol, 1 equiv) were dissolved in toluene (50 mL) in a 250 mL round-bottomed flask. The obtained reaction mixture was stirred for 12 h at 135 °C under N_2 atmosphere. Toluene was then removed *in vacuo* using a rotary evaporator, and the resulting solid was then recrystallized in hot methanol three times to give the compound **5** as a white solid. Yield: 90%. ^{1}H NMR (400MHz, $(CD_3)_2SO$, 25 °C, TMS), δ_{ppm}: 9.75 (s, 1H, OH), 7.04 (d, *J* = 8.9 Hz, 2H, ph), 6.82 (d, *J* = 8.8 Hz, 2H, ph), 6.36 (t, *J* = 3.6 Hz, 2H, CH=CH), 3.18 (t, *J* = 8.9 Hz, 2H, =CH-C***H***), 2.80 (d, *J* = 1.1 Hz, 2H, CHCON), 1.45 (d, *J* = 10.0 Hz, 1H, CH_2-bridge), 1.38 (d, *J* = 10.0 Hz, 1H, CH_2-bridge) Selected IR (KBr, cm^{-1}): 3356 (υ_{OH}), 2982, 1772 ($\upsilon_{CH=CH}$), 1691 ($\upsilon_{C=O}$), 1595, 1515, 1439 ($\upsilon_{CH=CH\ of\ ph}$), 1402, 1268, 1197, 791.

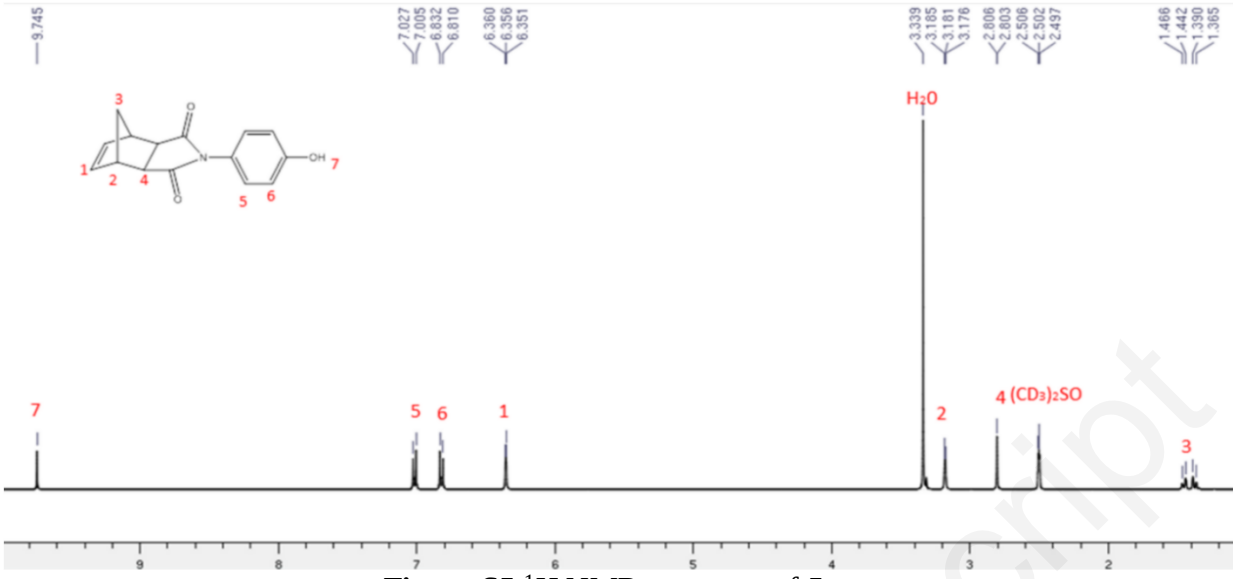

Figure S5 ^{1}H NMR spectrum of **5**.

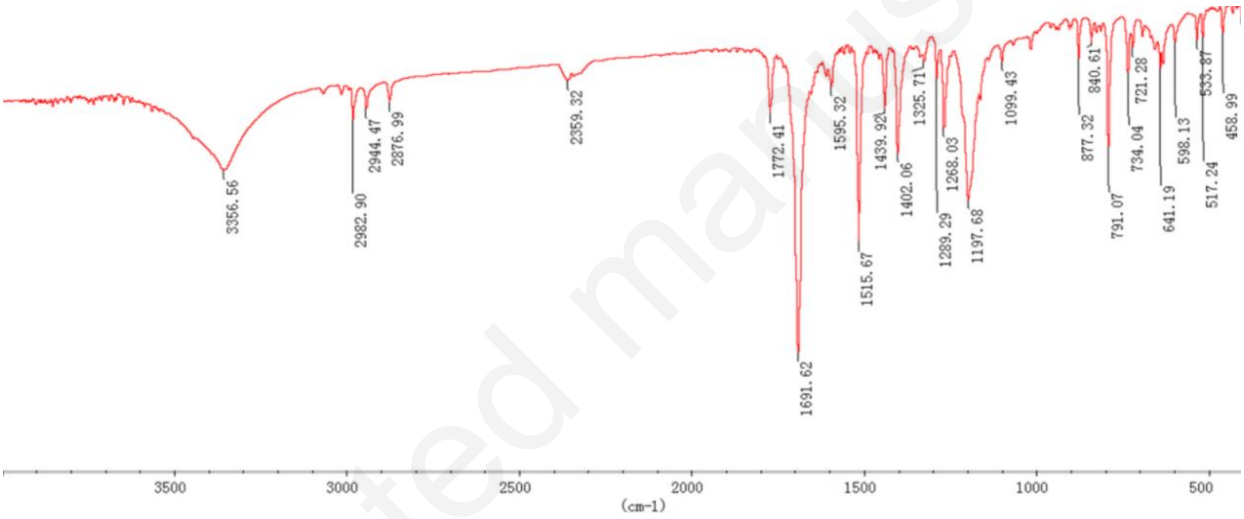

Figure S6 IR spectrum of **5**.

1.3. Synthesis of 6

1,8-Dibromooctane (55 g, 200 mmol, 10 equiv), potassium carbonate (K_2CO_3, 6.0 g, 43 mmol, 2 equiv) and acetonitrile (100 mL) were mixed and heated at 70 °C in a 500 mL round-bottomed flask. Then, compound **5** (5 g, 20 mmol, 1 equiv) in tetrahydrofuran (THF, 15 mL) was added dropwise into the above solution under stirring. After this addition, the reaction mixture was stirred at 75 °C for 12 h under N_2 atmosphere. All the solvents were then removed *in vacuo* using a rotary evaporator. The residue was dissolved in 50 mL of ethyl acetate, and the insoluble K_2CO_3 was removed by filtration. The solvent of the filtrate was removed *in vacuo* using a rotary evaporator, and the obtained residue was then purified by column chromatography with petroleum ether/ethyl acetate (10/1, v/v) as eluent. The

obtained white solid was further recrystallized in hot ethanol to give the compound **6** as transparent acicular crystals. Yield: 80%. ^{1}H NMR (400MHz, $(CD_3)_2SO$, 25 °C, TMS), δ_{ppm}: 7.14 (d, *J* = 8.7 Hz, 2H, ph), 7.00 (d, *J* = 8.7 Hz, 2H, ph), 6.36 (t, *J* = 3.7 Hz, 2H, CH=CH), 3.99 (t, *J* = 12.9 Hz, 2H, OCH_2), 3.53 (t, *J* = 13.5 Hz, 2H, CH_2Br), 3.19 (t, *J* = 3.2 Hz, 2H, =CHC***H***), 2.82 (d, *J* = 0.7 Hz, 2H, CHCON), 1.83-1.68 (m, 4H, C***H$_2$***CH_2Br and OCH_2C***H$_2$***), 1.47-1.30 (m, 10H, CH_2-bridge and 4 × CH_2). Selected IR (KBr, cm^{-1}): 3445(υ_{H2O}), 2937, 2360, 2341, 1704 ($\upsilon_{C=O}$), 1510, 1472 ($\upsilon_{CH=CH\ of\ ph}$), 1392, 1245, 1195, 793, 688.

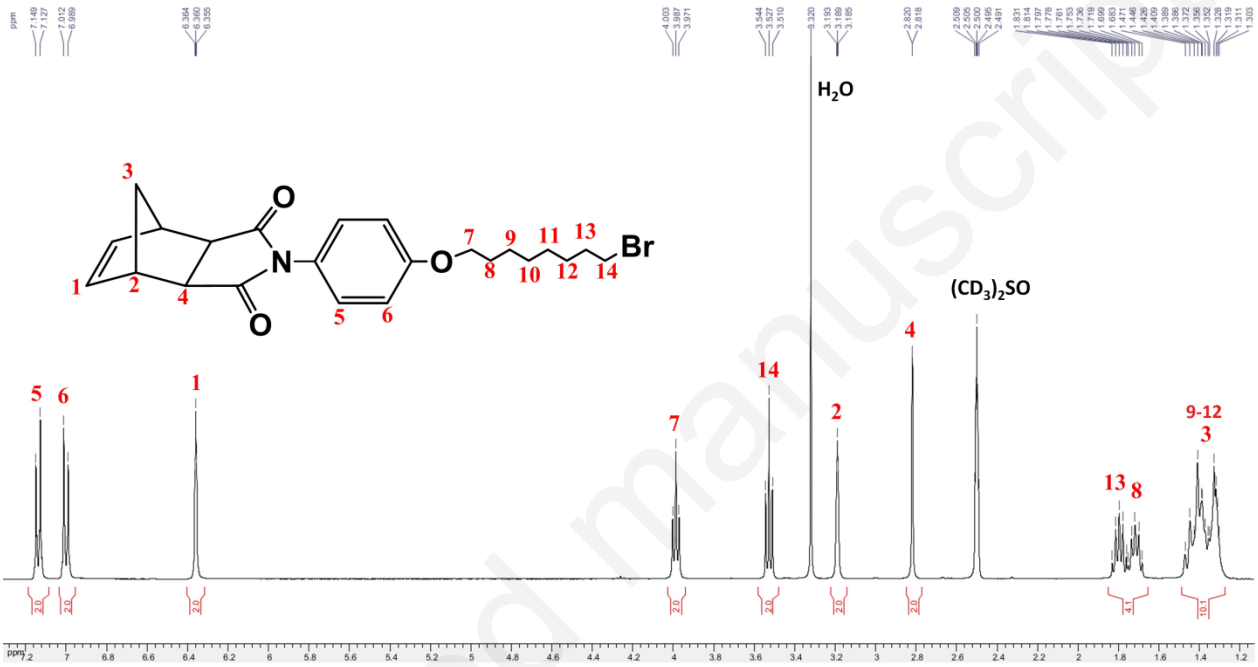

Figure S7 ^{1}H NMR spectrum of **6**.

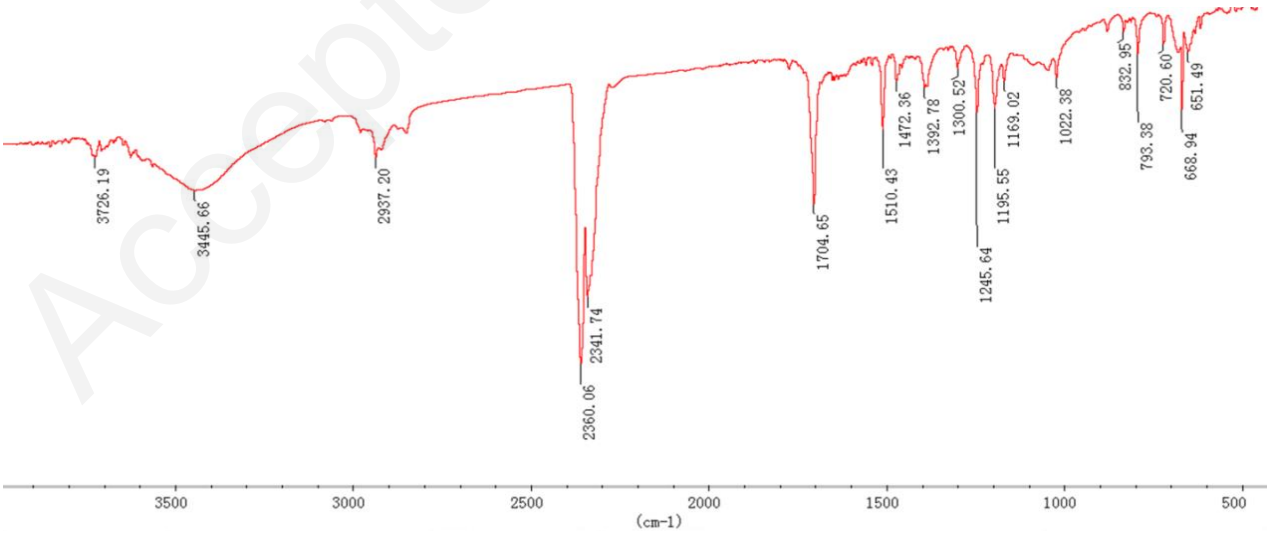

Figure S8 IR spectrum of **6**.

1.4. Synthesis of the monomer 7

Compounds **3** (5.0 g, 17 mmol, 1 equiv) and **6** (7.4 g, 17 mmol, 1 equiv) were dissolved in acetonitrile (100 mL) in a 500-mL round-bottomed flask. The reaction mixture was stirred at 75 °C for 12 h under N_2 atmosphere. Then, acetonitrile was removed *in vacuo* using a rotary evaporator. The residue was purified by precipitation from CH_2Cl_2 (50 mL) with ethyl ether (150 mL), and the precipitation procedure was repeated five times to give the pure quaternary ammonium monomer **7** as a yellow solid. Yield: 70%.

Synthesis of homopolymer 8

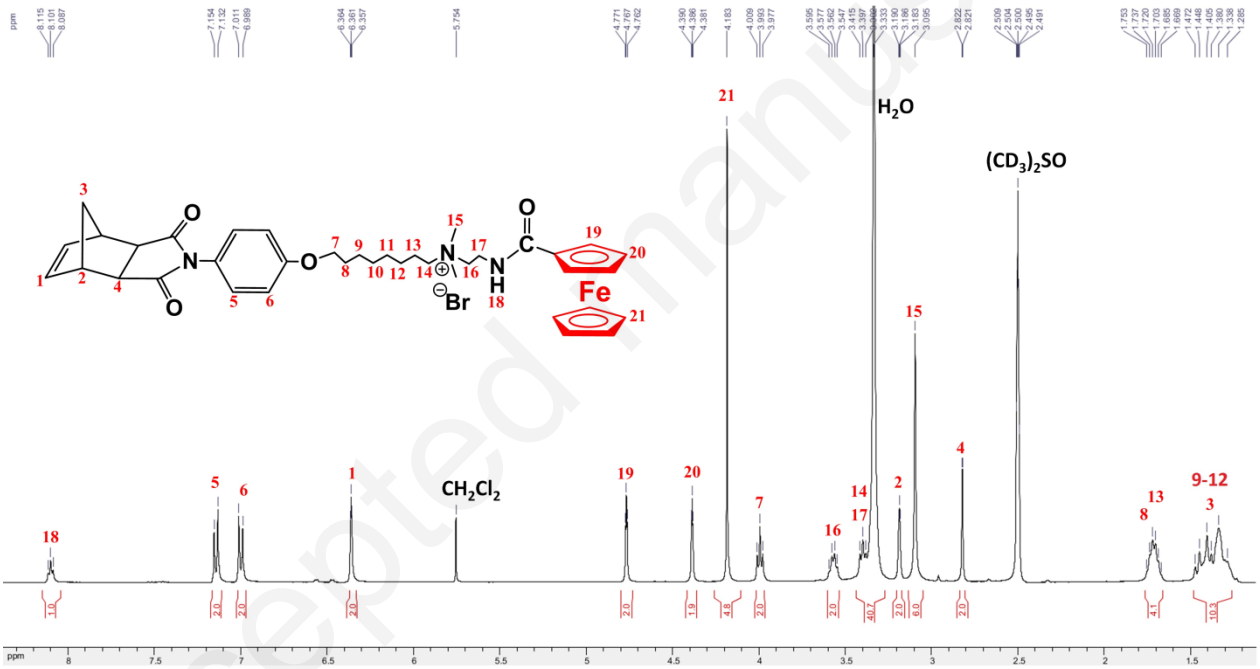

Figure S9 ^{1}H NMR spectrum of **7**.

^{1}H NMR (400MHz, $(CD_3)_2SO$, 25 °C, TMS), δ_{ppm}: 8.10 (t, *J* = 11.2 Hz, 1H, NHCO), 7.14 (d, *J* = 8.8 Hz, 2H, ph), 7.00 (d, *J* = 8.8 Hz, 2H, ph), 6.36 (t, *J* = 3.2 Hz, 2H, CH=CH), 4.77 (t, *J* = 3.7 Hz, 2H, sub. Cp), 4.39 (t, *J* = 3.5 Hz, 2H, sub. Cp), 4.18 (s, 5H, free Cp), 3.99 (t, *J* = 12.6 Hz, 2H, OCH_2), 3.59-3.55 (q, 2H, $NCH_2C\boldsymbol{H_2}NHCO$), 3.42-3.33 (m, $C\boldsymbol{H_2}N(CH_3)_2C\boldsymbol{H_2}$ and H_2O), 3.19 (t, *J* = 2.9 Hz, 2H, =CHC***H***), 3.09 (s, 6H, $N(CH_3)_2$), 2.82 (d, *J* = 0.6 Hz, 2H, CHCON), 1.75-1.66 (m, 4H, $C\boldsymbol{H_2}CH_2N(CH_3)_2$ and $OCH_2C\boldsymbol{H_2}$), 1.47-1.28 (m, 10H, CH_2-bridge and 4 × CH_2).

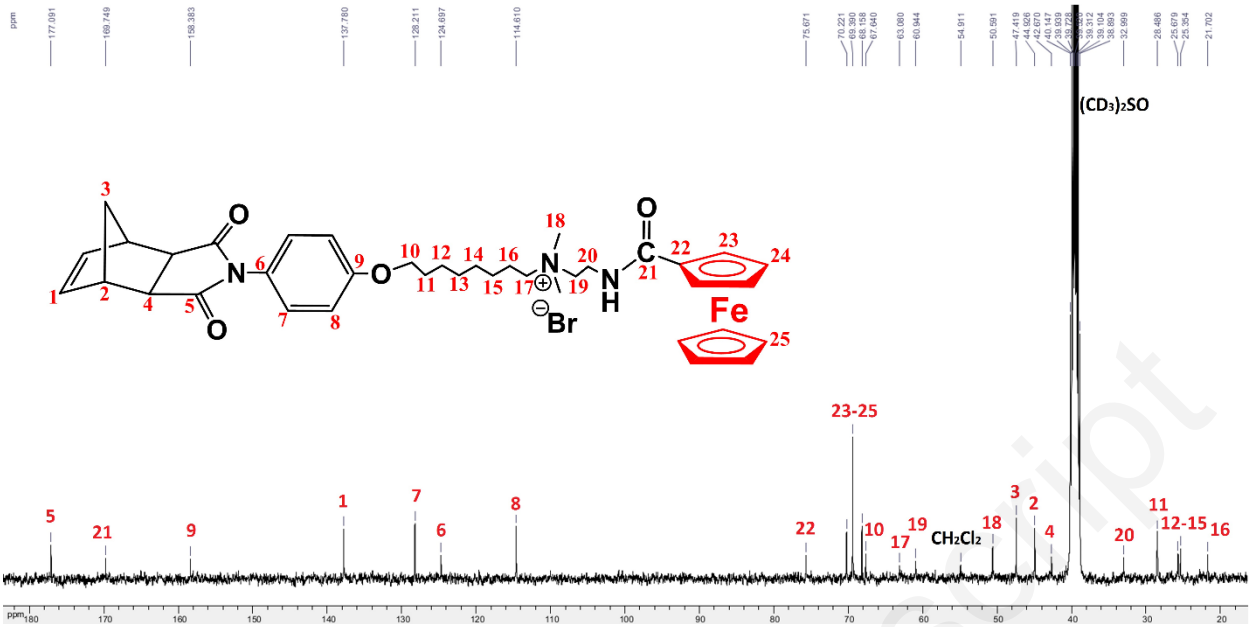

Figure S10 ^{13}C NMR spectrum of **7** in $(CD_3)_2SO$.

^{13}C NMR (100MHz, $(CD_3)_2SO$, 25 °C, TMS), δ_{ppm}: 177.6 (NC=O), 170.2 (NHC=O), 158.9 (ph), 138.3 (CH=CH), 128.7 (ph), 125.2 (ph), 115.1 (ph), 76.2, 70.7, 69.9, 68.7 (Cp), 68.1 (OCH_2), 63.6 (NCH_2), 61.5 (NCH_2CH_2NH), 55.5 (NCH_3), 51.1 (CH_2-bridge), 47.9 (=CHCH), 45.4 (CHCON), 43.2 (NCH_2CH_2NH), 40.6, 33.5, 29.0, 26.2, 25.9, 22.2 (CH_2).

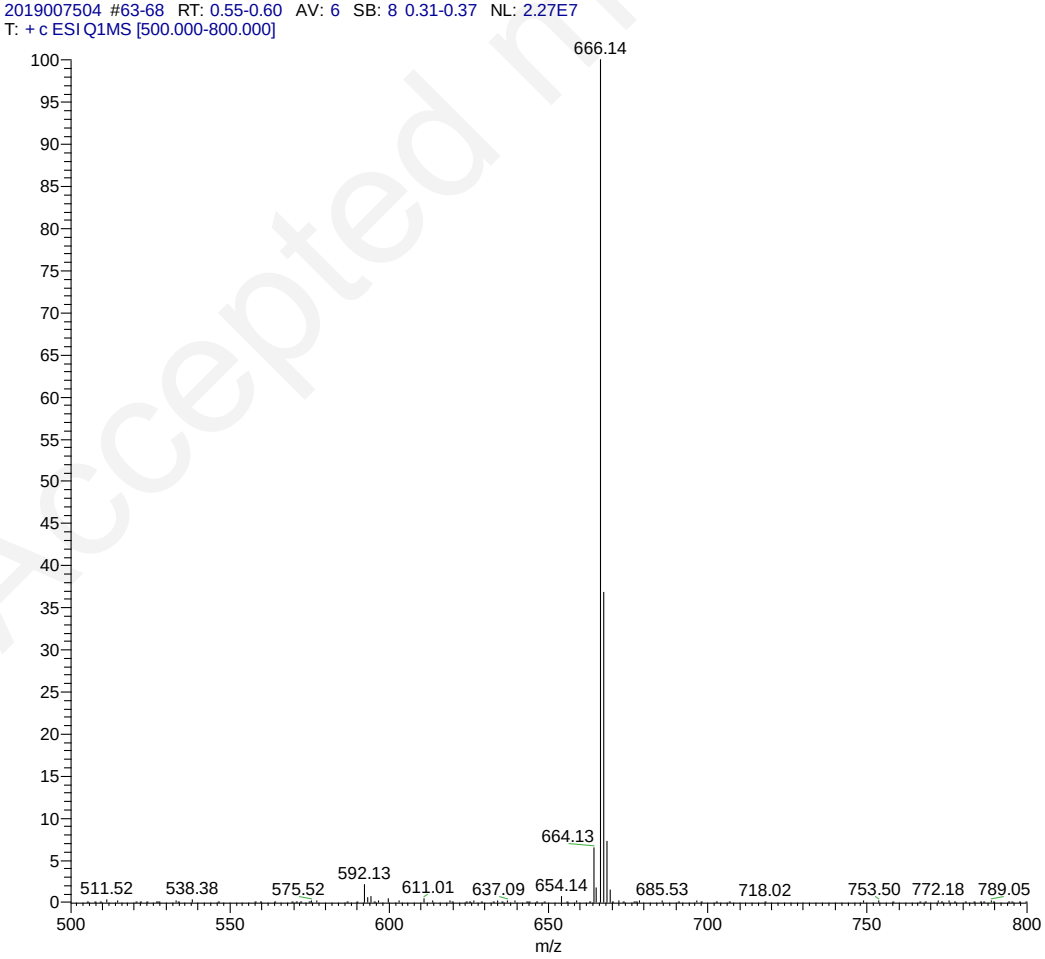

Figure S11 Mass spectrum of **7**.

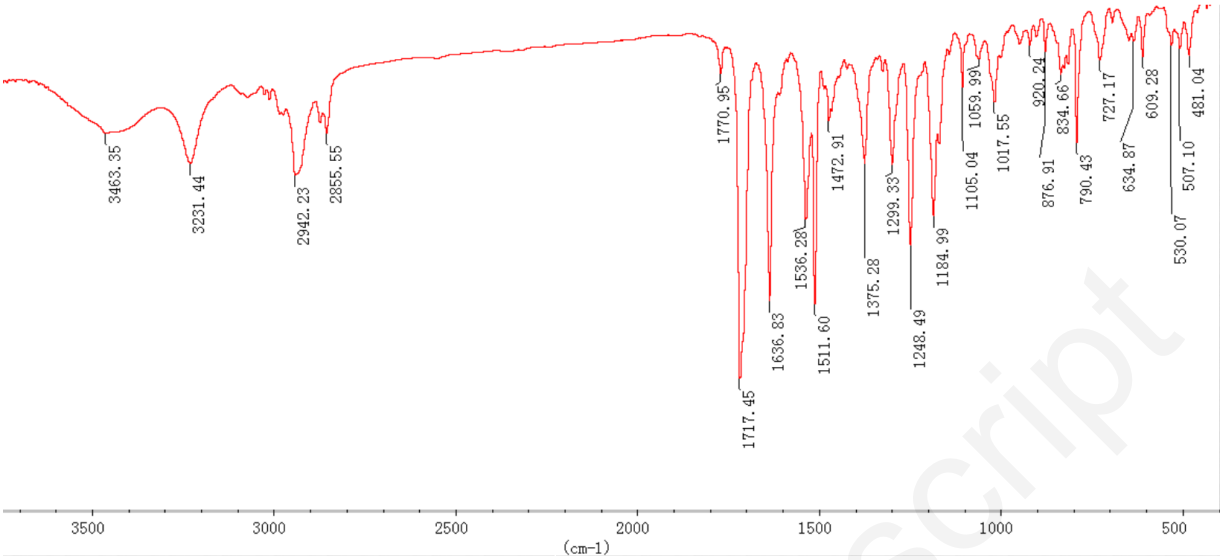

Figure S12 IR spectrum of **7**.

3231 (υ_{NH}), 2942 (υ_{CH2}), 1770 ($\upsilon_{CH=CH}$), 1717 ($\upsilon_{NC=O}$), 1636 ($\upsilon_{NHC=O}$), 1536, 1511, 1472 ($\upsilon_{CH=CH\ of\ ph}$), 1375, 1299, 1248, 1184, 1017, 834 (υ_{FeII}), 790.

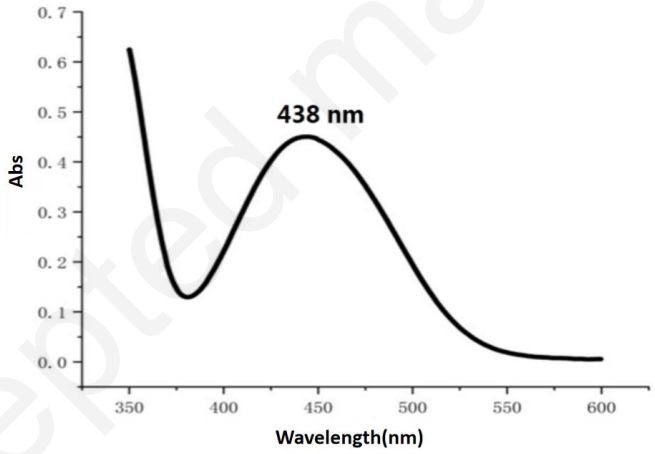

Figure S13 UV-vis spectrum of **7** in H_2O.

1.5. Synthesis of the homopolymer 8

Four feed molar ratios (monomer **7**: catalyst A), namely 10:1, 25:1, 50:1 and 100:1, were adopted to synthesize the homopolymers **8** with the desired polymerization degrees of 10, 25, 50 and 100, respectively. The general procedure is as follows: monomer **7** (0.2 g, 0.268 mmol) was dissolved in 2 mL of dry DMF at room temperature (RT, 25 °C). The required catalyst A (see Scheme 1) was freshly prepared following the reported method,[40] and dissolved in 0.1 mL of dry DMF under N_2 atmosphere. The above DMF solution of **7** was

then injected at RT using a syringe into the catalyst solution under stirring condition. The obtained mixture was agitated vigorously for 30 min at RT under N_2 atmosphere, and EVE (2 mL) was added to terminate the polymerization. Diethyl ether (Et_2O, 10 mL) was added into the final solution, and the homopolymer **8** was separated as a yellowish-brown powdered precipitate, washed 5 times using Et_2O (5 × 10 mL) for purification, and dried at RT under reduced pressure.

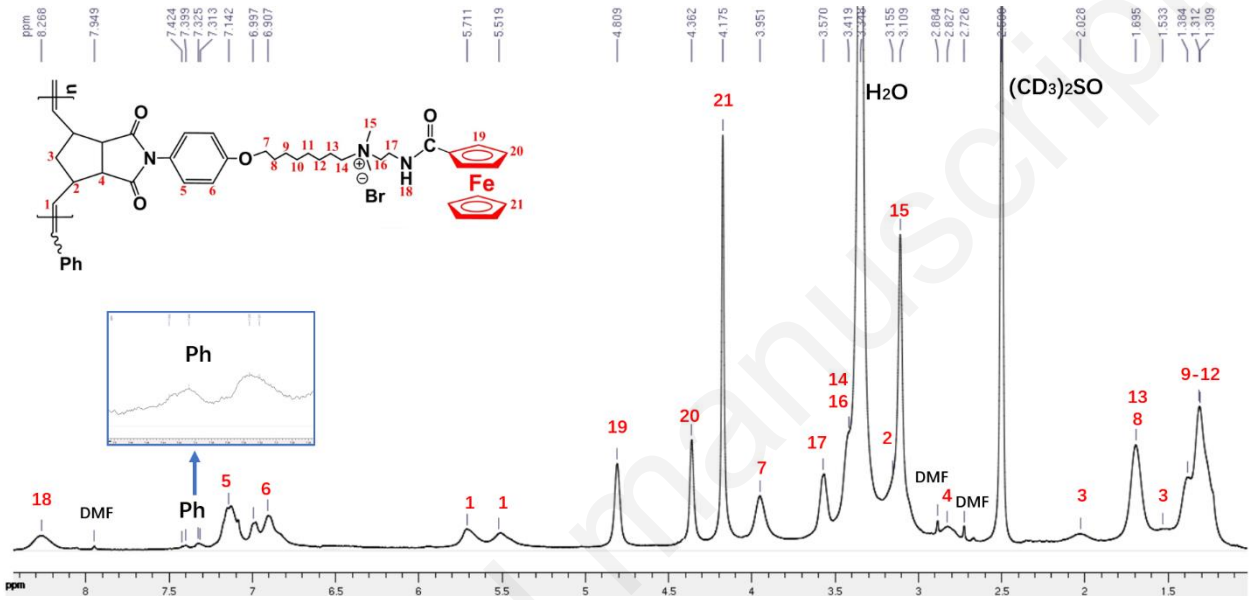

Figure S14 ^{1}H NMR spectrum of **8a** in $(CD_3)_2SO$.

^{1}H NMR (400 MHz, $(CD_3)_2SO$, 25 °C, TMS), δ_{ppm}: 8.26 (broad, 1H, NHCO), 7.42-7.31 (m, end-ph), 7.14-6.90 (m, 4H, ph), 5.71 and 5.51 (double broad, 2H, CH=CH), 4.81 (s, 2H, sub. Cp), 4.36 (s, 2H, sub. Cp), 4.17 (s, 5H, free Cp), 3.95 (broad, 2H, OCH_2), 3.57 (broad, 2H, NCH_2CH_2NHCO), 3.49-3.34 (m, $CH_2N(CH_3)_2CH_2$ and H_2O), 3.11 (s, =CHCH and $N(CH_3)_2$), 2.72 (broad, CHCON), 2.03 (broad, CH_2 of cyclopentane), 1.69 (broad, 4H, $CH_2CH_2N(CH_3)_2$ and OCH_2CH_2), 1.53 (broad, CH_2 of cyclopentane), 1.39 and 1.31 (broad, 8H, 4 × CH_2).

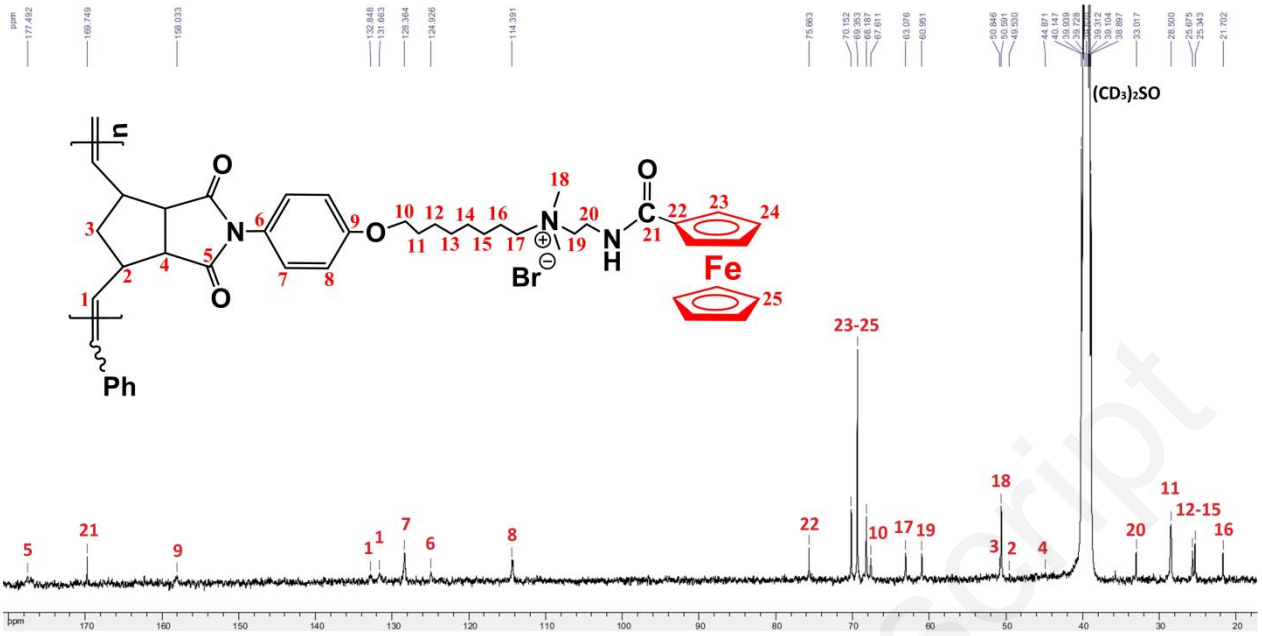

Figure S15 ^{13}C NMR spectrum of **8a** in $(CD_3)_2SO$.

^{13}C NMR (100MHz, $(CD_3)_2SO$, 25 °C, TMS), δ_{ppm}: 177.4 (NC=O), 169.7 (NHC=O), 158.0 (ph), 132.8 and 131.6 (CH=CH), 128.3 (ph), 124.9 (ph), 114.3 (ph), 75.6, 70.1, 69.3, 68.1 (Cp), 67.6 (OCH_2), 63.1 (NCH_2), 60.9 (NCH_2CH_2NH), 50.8 (CH_2 of cyclopentane), 50.6 (NCH_3), 49.5 (=CHCH), 44.9 (CHCON), 33.0 (NCH_2CH_2NH), 28.5 (OCH_2CH_2), 25.7, 25.3 (CH_2), 21.7 ($CH_2CH_2N^+$).

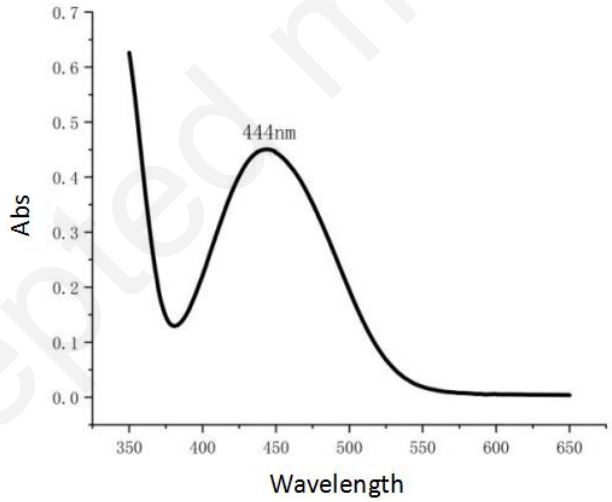

Figure S16 UV-vis spectrum of **8a** in H_20.

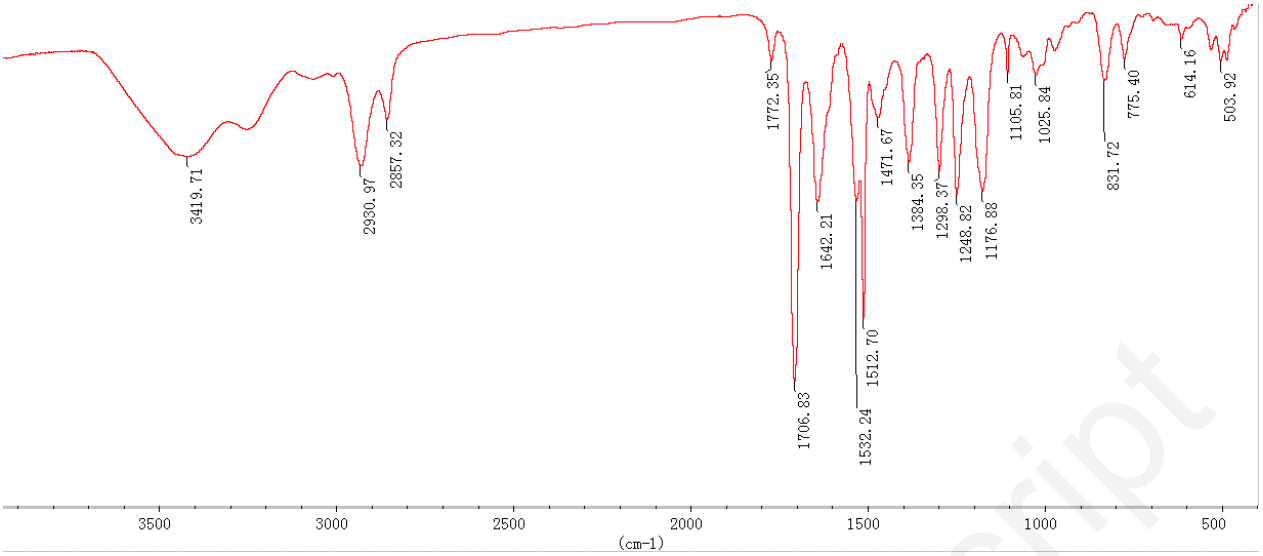

Figure S17 IR spectrum of **8a**.

3419 (υ_{NH}), 2930 (υ_{CH2}),2857, 1772 ($\upsilon_{CH=CH}$), 1706 ($\upsilon_{NC=O}$), 1642 ($\upsilon_{NHC=O}$), 1532, 1512, 1471 ($\upsilon_{CH=CH\ of\ ph}$), 1384, 1298, 1248, 1176, 1105, 1025, 831 (υ_{FeII}), 775.

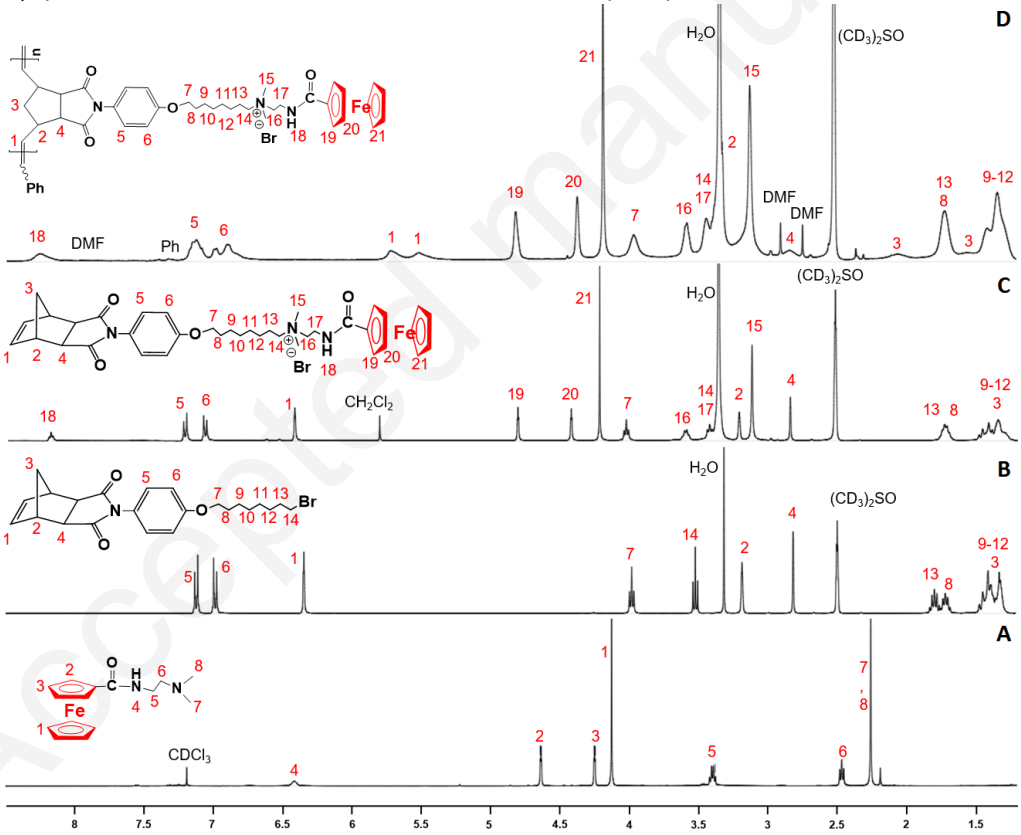

Figure S18 ^{1}H NMR spectra of compounds 3 (A), 6 (B), 7 (C) and 8 (D)

2. Cyclic voltammetry (CV)

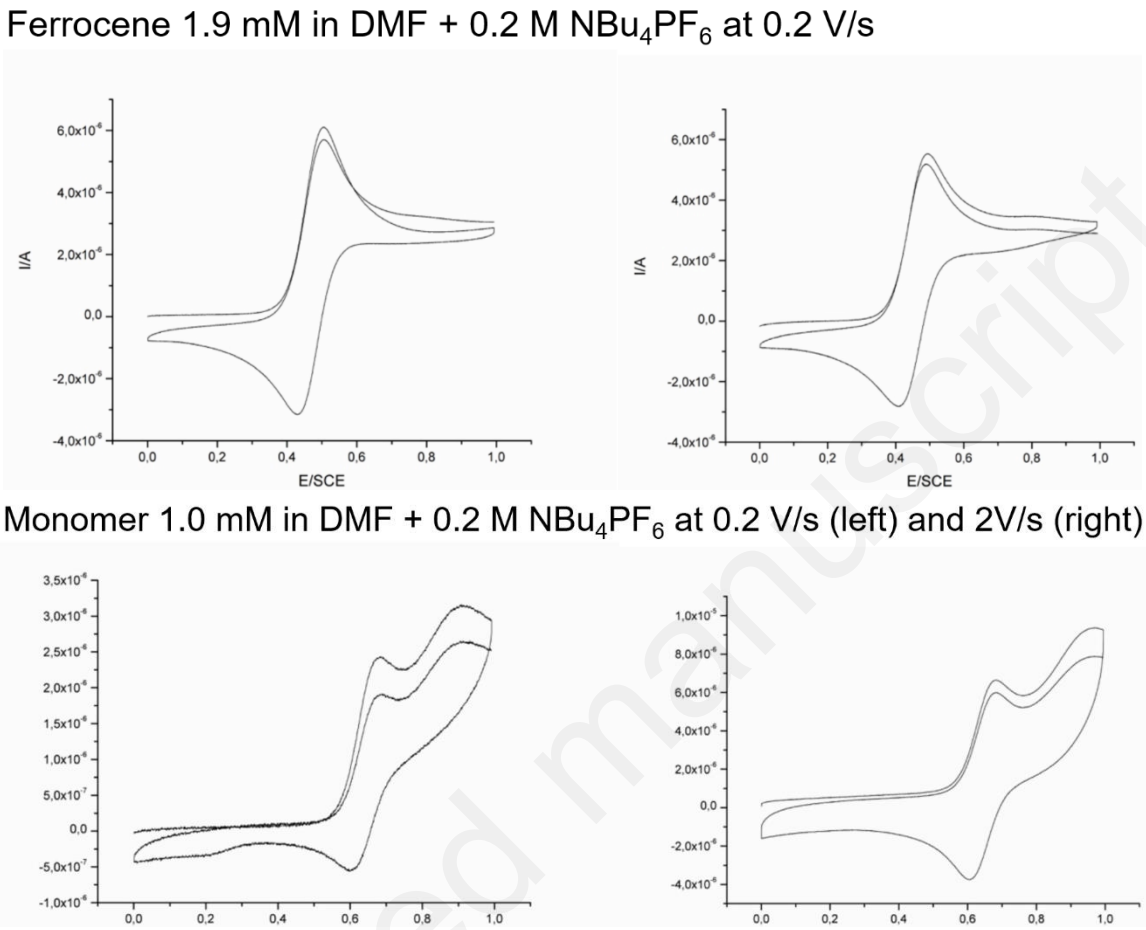

Figure S19 CV curves of ferrocene and monomer **7** in DMF. Conditions: Ferrocene (0.0018 g) was dissolved in 5 mL of dimethylformamide (DMF), and its concentration was 1.94×10^{-3} mol L^{-1}. Monomer **7** (0.0038 g) was dissolved in 5 mL of DMF, and its concentration was 1.02×10^{-3} mol L^{-1}. The supporting salt is tetrabutylammonium hexafluorophosphate (NBu_4PF_6), and its concentration in DMF is 0.2 mol L^{-1}. Working electrode: glassy carbon electrode, 1 mm. Counter electrode: platinum electrode. Reference electrode: calomel electrode.

Table S1 CV Data of ferrocene and monomer **7** in DMF

	$E_{1/2}$ (V/SCE)	ΔE_p (V)	Ip (μA)
Monomer **7**	0.64	0.08	6.5
Ferrocene	0.47	0.07	6.1

Note: CV curve of monomer **7** was measured at scan rate of 2 V/s, while the CV curve of ferrocene was determined at the scan rate of 0.2 V/s.

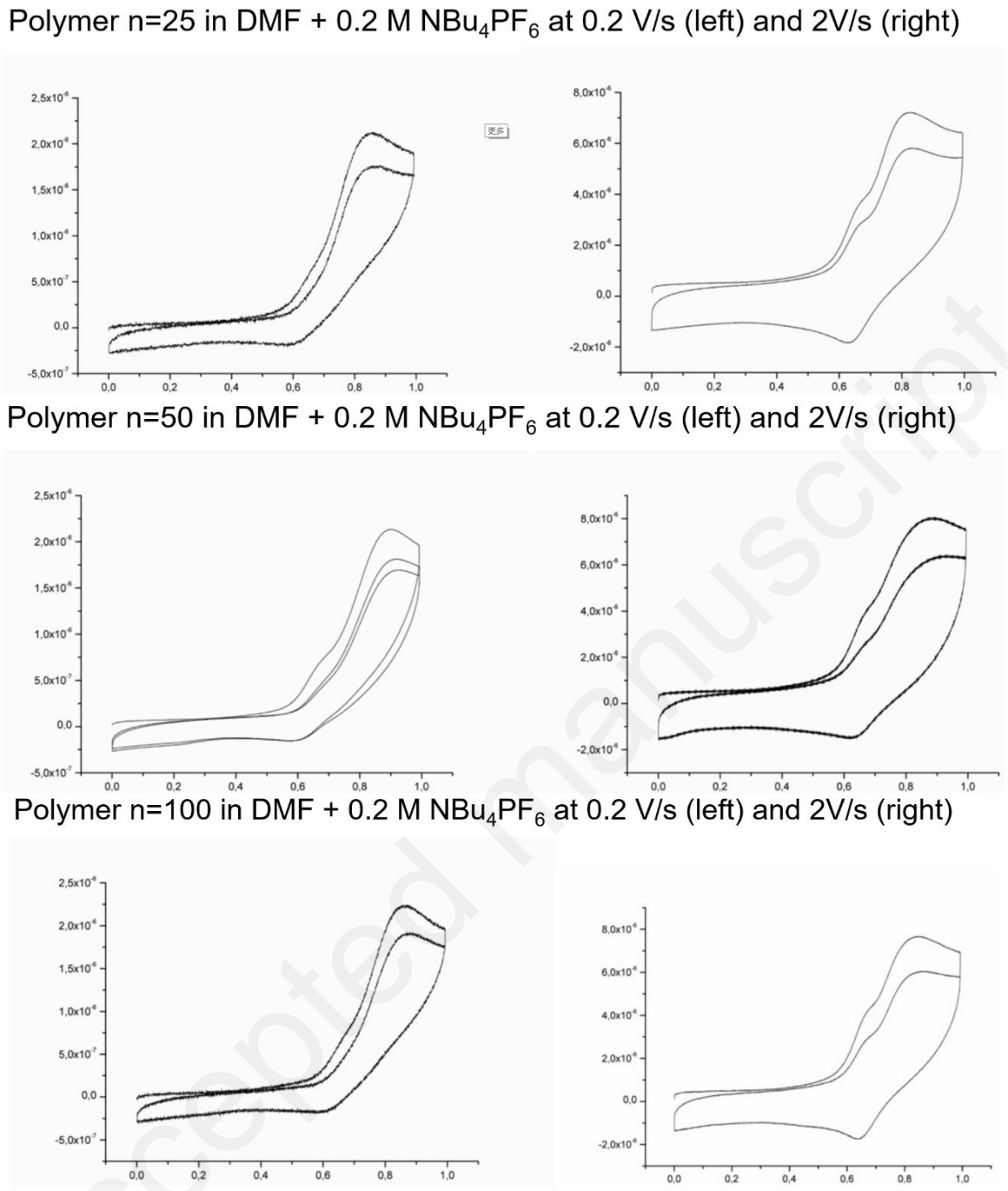

Figure S20 CV curves of homopolymers **8b-d** in DMF. Conditions: **8b** (0.0038 g, n=25), **8c** (0.0039 g, n=50) and **8d** (0.0038, n=100) were dissolved, respectively, in 5 mL of DMF. The supporting salt is tetrabutylammonium hexafluorophosphate (NBu_4PF_6), and its concentration in DMF is 0.2 mol L^{-1}. Working electrode: glassy carbon electrode, 1 mm. Counter electrode: platinum electrode. Reference electrode: calomel electrode.

Table S2 CV Data of homopolymers **8b-d** in DMF (scan rate: 2V/s)

	$E_{1/2}$ (V/SCE)	ΔE_p (V)	Ip (μA)
8b (n=25)	0.72	0.160	3.6
8c (n=50)	0.76	0.230	4.0
8d (n=100)	0.76	0.200	4.1

3. Kinetic study and end-group analysis

3.1. Kinetic study

The polymerization of monomer **7** was monitored by using *in situ* ^{1}H NMR spectroscopy method. The kinetic study of **7** for the synthesis of **8a** was used as an example to show the general procedure. Concretely, monomer **7** (0.2 g, 0.268 mmol, 10 equiv) was dissolved in 2 mL of dry DMF. And the obtained solution was then added using a syringe into the DMF solution (0.1 mL) of freshly prepared catalyst A (23.73 mg, 0.00268 mmol, 1 equiv) under N_2 atmosphere and stirring condition. The obtained mixture was then stirred dramatically at RT under N_2 atmosphere. After 5, 15, 30, 60, 120 and 180 min of stirring, respectively, 0.1 mL of reaction mixture was taken out using a syringe, quenched by adding 0.1 mL of EVE, and dried under reduced pressure. Then, the ^{1}H NMR spectrum of the dried reaction mixture was determined using $(CD_3)_2SO$ as the solvent. When the peak at 6.36 ppm disappeared completely, the polymerization of monomer **7** was deemed to be accomplished with the conversion ratio of 100%. As shown in Figure S20, after 30 min of stirring, there is no peak at 6.36 ppm corresponding to the olefinic protons (CH=CH) of monomer **7**, and two broad peaks at 5.72 and 5.51 ppm, assigned to the olefinic protons of polynorbornene, were observed. These results indicate that all the polymerizations for the synthesis of homopolymers **8a-d** can be achieved in 30 min.

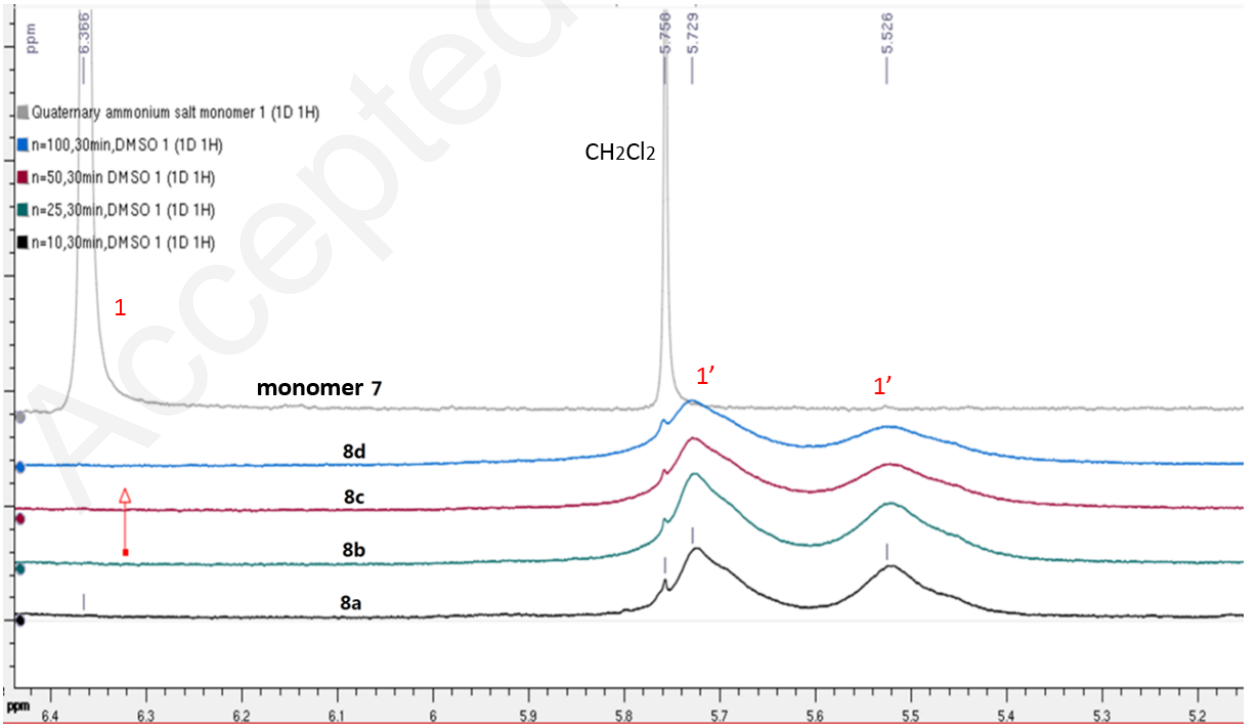

Figure S21 Partial ^{1}H NMR spectra of monomer **7** and the reaction mixtures for the synthesis of homopolymers **8a-d** after stirring of 30 min. Note: The peak marked by 1 is the original

CH=CH protons of monomer **7**, and the two peaks labeled by 1' are from the CH=CH protons of polynorbornene framework.

3.2. Calculation of polymer degrees for homopolymers 8a-d by ^{1}H NMR end-group analysis

Table S3 Polymer degree of homopolymer **8a** by using ^{1}H NMR end-group analysis[a]

Proton peak	End-ph	NHCO	CH=CH	Sub. Cp	Sub. Cp	OCH_2	$N(CH_3)_2$
δ_{ppm}	7.313-7.424	8.268	5.519 and 5.711	4.809	4.362	3.951	3.109
Integration	0.411-0.426	0.911-0.926	1.803-1.870	1.715-1.652	1.704-1.543	1.807-1.825	5.360-5.401
n_{p2a}[b]	-	10-11	10-11	9-10	9-10	10-11	10-11
n_{p2b}[c]		10 ± 1					

[a] Figure S14 was used for the calculation of the polymer degree of **8a**. [b] Calculated polymer degrees based on integral of each peak. [c] Average polymer degree according to n_{p2a} values.

As shown in Table S3, the ^{1}H NMR end-group analysis in (CD3)2SO of homopolymer 8a provided the value of 10 ± 1 for the polymer degree of 8a. These calculations were conducted by comparing the intensities of the signals of the five protons of the end-phenyl group with those of characteristic protons in the homopolymer 8a. Concretely, the proton integration for end-phenyl group (7.313-7.424 ppm) was compared with those of the NHCO group (8.268 ppm), olefinic protons (CH=CH, 5.519 and 5.711 ppm) of polynorbornene, substituted Cp protons (4.809 and 4.362 ppm), OCH2 proton (3.951 ppm) and methyl ($N(CH_3)_2$, 3.109 ppm) groups, respectively. The obtained corresponding values are 10-11, 10-11, 9-10, 9-10, 10-11 and 10-11, respectively. Thus, the average value of the polymer degree is 10 ± 1. The error is due to the integration error on each signal.

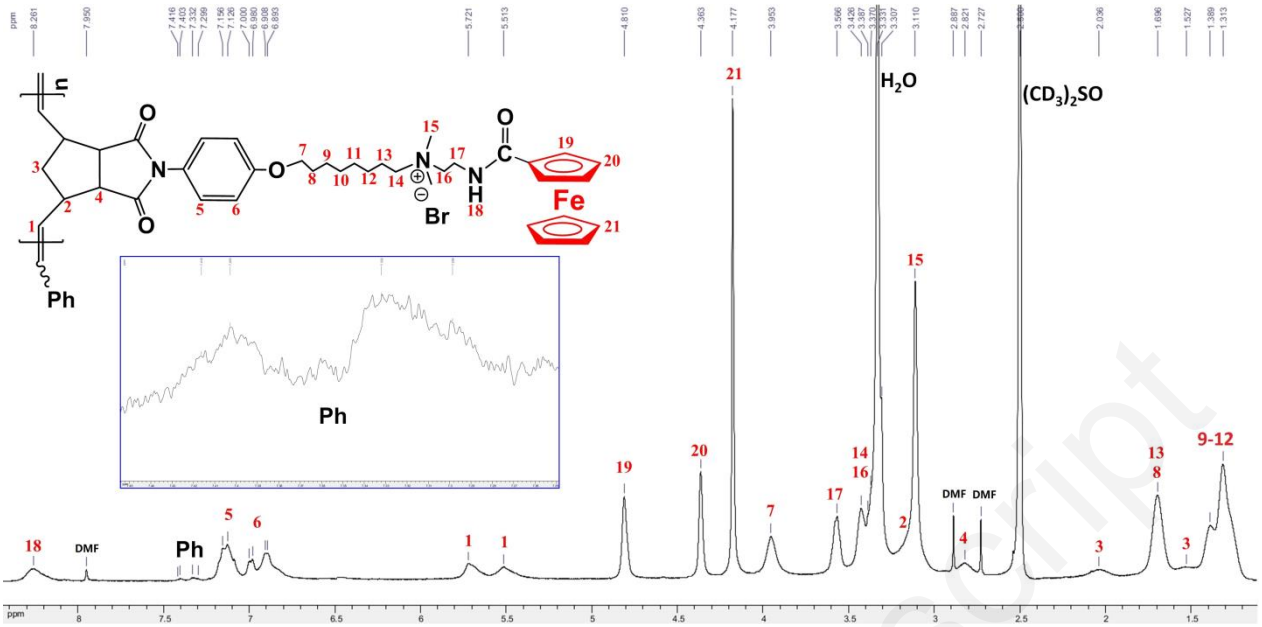

Figure S22 ^{1}H NMR (400 MHz) spectrum of **8b** in $(CD_3)_2SO$.

Table S4 Polymer degree of homopolymer **8b** by using ^{1}H NMR end-group analysis[a]

Proton peak	End-ph	NHCO	CH=CH	Sub. Cp	Sub. Cp	OCH_2	$N(CH_3)_2$
δ_{ppm}	7.416-7.299	8.261	5.721 and 5.513	4.810	4.363	3.953	3.110
Integration	0.188-0.193	1.013-1.015	2.005-2.047	1.913-1.955	1.762-1.833	1.829-1.931	5.431-5.527
n_{p2a}[b]	-	26-27	26-27	25-26	23-24	24-26	23-24
n_{p2b}[c]		25 ± 2					

[a] Figure S21 was used for the calculation of the polymer degree of **8b**. [b] Calculated polymer degrees based on integral of each peak. [c] Average polymer degree according to n_{p2a} values.

As shown in Table S4, the ^{1}H NMR end-group analysis in $(CD_3)_2SO$ of homopolymer **8b** provides the value of 25 ± 2 for the polymer degree of **8b**. These calculations were conducted by comparing the intensities of the signals of the five protons of the end-phenyl group with those of characteristic protons in the homopolymer **8b**. Concretely, the proton integration for end-phenyl group (7.416-7.299 ppm) was compared with those of the NHCO group (8.261 ppm), olefinic protons (CH=CH, 5.721 and 5.513 ppm) of polynorbornene, substituted Cp protons (4.810 and 4.363 ppm), OCH_2 proton (3.953 ppm) and methyl ($N(CH_3)_2$, 3.110 ppm) groups, respectively. The obtained corresponding values are 26-27, 26-27, 25-26, 23-24, 24-26 and 23-24, respectively. Thus, the average value of the polymer degree is 25 ± 2. The error is due to the integration error on each signal.

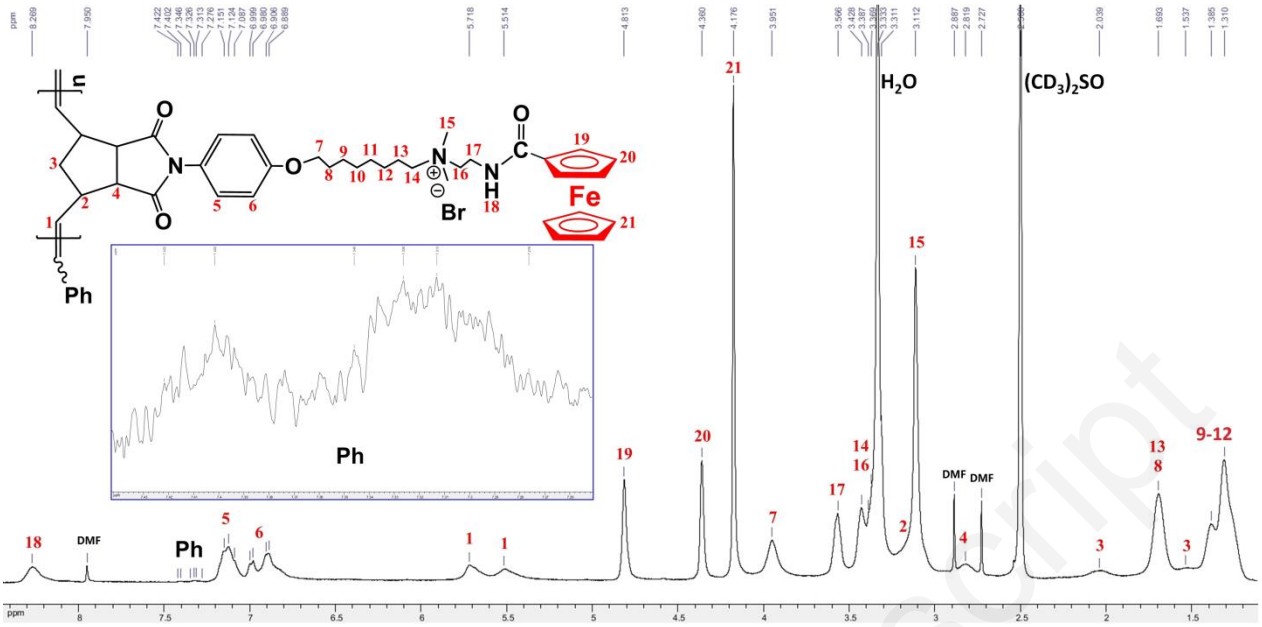

Figure S23 ^{1}H NMR (400 MHz) spectrum of **8c** in $(CD_3)_2SO$.

Table S5. Polymer degree of homopolymer **8c** by using ^{1}H NMR end-group analysis[a]

Proton peak	End-ph	NHCO	CH=CH	Sub. Cp	Sub. Cp	OCH_2	$N(CH_3)_2$
δ_{ppm}	7.422-7.276	8.269	5.718 and 5.514	4.183	4.360	3.951	3.112
Integration	0.093-0.098	0.920-0.934	1.950-1.996	1.963-1.924	1.932-1.957	1.913-1.34	5.479-5.512
n_{p2a}[b]	-	47-50	50-53	50-52	49-52	49-52	47-49
n_{p2b}[c]		50 ± 3					

[a]Figure S22 was used for the calculation of the polymer degree of **8c**. [b]Calculated polymer degrees based on integral of each peak. [c]Average polymer degree according to n_{p2a} values.

As shown in Table S5, the ^{1}H NMR end-group analysis in $(CD_3)_2SO$ of homopolymer **8c** provides the value of 50 ± 3 for the polymer degree of **8c**. These calculations were conducted by comparing the intensities of the signals of the five protons of the end-phenyl group with those of characteristic protons in the homopolymer **8c**. Concretely, the proton integration for end-phenyl group (7.422-7.276 ppm) was compared with those of the NHCO group (8.269 ppm), olefinic protons (CH=CH, 5.718 and 5.514 ppm) of polynorbornene, substituted Cp protons (4.183 and 4.360 ppm), OCH_2 proton (3.951 ppm) and methyl ($N(CH_3)_2$, 3.112 ppm) groups, respectively. The obtained corresponding values are 47-50, 50-53, 50-52, 49-52, 49-52 and 47-49, respectively. Thus, the average value of the polymer degree is 50 ± 3. The error is due to the integration error on each signal.

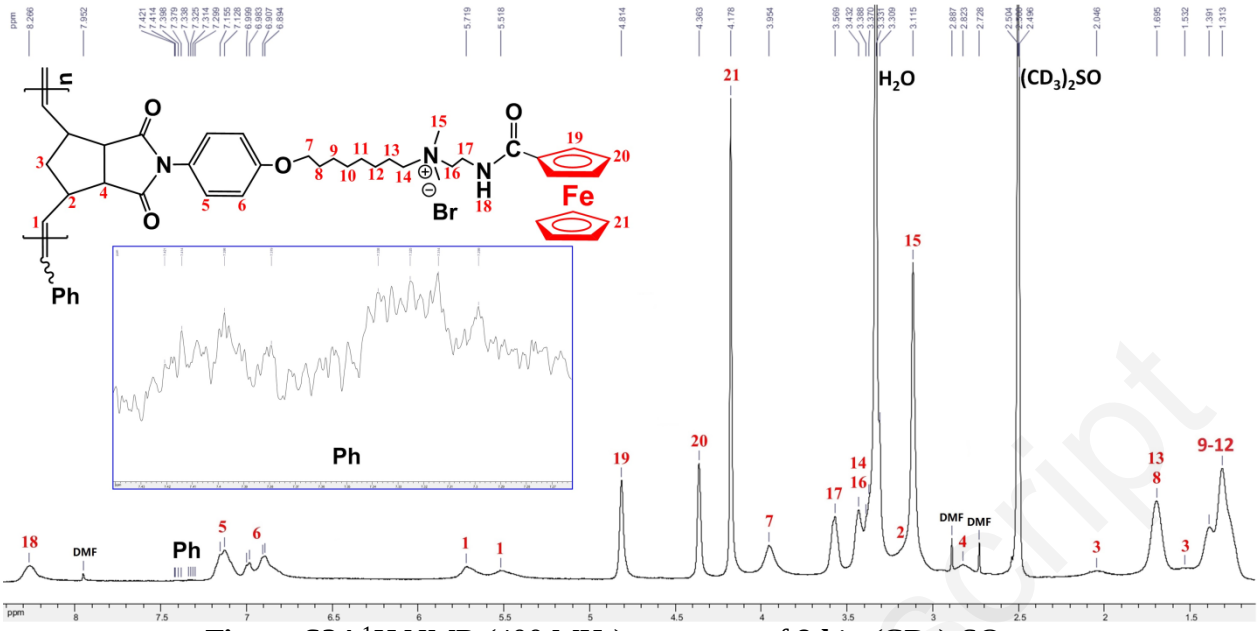

Figure S24 ^{1}H NMR (400 MHz) spectrum of **8d** in $(CD_3)_2SO$.

Table S6. Polymer degree of homopolymer **8d** by using ^{1}H NMR end-group analysis[a]

Proton peak	End-ph	CH=CH	Sub. Cp	Sub. Cp	OCH_2	$N(CH_3)_2$	8-CH_2 and 13-CH_2
δ_{ppm}	7.421-7.379	5.719 and 5.518	4.814	4.363	3.954	3.115	1.695
Integration	0.081-0.088	2.758-2.886	2.698-2.732	2.837-2.898	2.741-2.819	5.543-8.728	5.461-5.484
n_{p2a}[b]	-	78-89	77-84	81-89	78-87	81-89	78-85
n_{p2b}[c]		83 ± 6					

[a]Figure S23 was used for the calculation of the polymer degree of **8d**. [b]Calculated polymer degrees based on integral of each peak. [c]Average polymer degree according to n_{p2a} values.

As shown in Table S6, the ^{1}H NMR end-group analysis in $(CD_3)_2SO$ of homopolymer **8d** provides the value of 83 ± 6 for the polymer degree of **8d**. These calculations were conducted by comparing the intensities of the signals of the five protons of the end-phenyl group with those of characteristic protons in the homopolymer **8d**. Concretely, the proton

integration for end-phenyl group (7.421-7.379 ppm) was compared with those of the olefinic protons (CH=CH, 5.719 and 5.518 ppm) of polynorbornene, substituted Cp protons (4.814 and 4.363 ppm), OCH_2 proton (3.954 ppm), methyl ($N(CH_3)_2$, 3.115 ppm) and 8-CH_2 and 13-CH_2 (1.695 ppm) groups , respectively. The obtained corresponding values are 78-89, 77-84, 81-89, 78-87, 81-89 and 78-85, respectively. Thus, the average value of the polymer degree is 83 ± 6. The error is due to the integration error on each signal.

4. Solubility of the monomer 7 and the homopolymers 8.

Table S7 Solubility of **7** and **8a-d** in different solvents

	H_2O	CH_2Cl_2	Methanol	Petroleum ether	DMF	THF	DMSO
Monomer **7**	√	√	√	--	√	√	√
Homopolymer **8a**	√	○	√	--	√	√	√
Homopolymer **8b**	○	--	√	--	√	○	√
Homopolymer **8c**	○	--	○	--	√	○	√
Homopolymer **8d**	○	--	--	--	√	--	√

Note:√: Easily soluble, ○: Partially soluble; --: Insoluble.

Test method: 5 mg sample was added in 1 mL solvent, and stirred dramatically at room temperature, and then allowed to stand for 6h. Then the filter residue was filtered with a syringe filter with a pore size of 220 nm. The solubility of sample was evaluated by the amount of filter residue.

5. Redox properties of the monomer 7 and the homopolymer 8

The oxidation-reduction cycle experiment of the monomer 7: Monomer **7** (10 mg, 0.0134 mmol) was firstly dissolved in 2 mL of deionized water, and the UV-vis spectrum of the formed solution was determined. Then, the equimolar solid ferric trichloride ($FeCl_3$) (2.17mg, 0.0134mmol) was added as an oxidizing agent into the aqueous solution, and stirred acutely at RT until the color of solution changed from original orange to green. The green solution was detected by using UV-vis spectroscopy. Next, the equimolar L-sodium ascorbate solution (2.66mg, 0.0134mmol) was adopted as a reducing agent and added into the green solution. The vigorous stirring was then conducted at RT until the color of the solution change from green to yellow. Finally, the UV-vis spectrum of the reduced solution was recorded.

The oxidation-reduction cycle experiment of the homopolymer 8a: homopolymer **8a** (10 mg, 0.0134 mmol) was firstly dissolved in 2 mL of deionized water, and the UV-vis spectrum of the formed solution was determined. Then, the equimolar ferric trichloride solid ($FeCl_3$)

(2.17mg, 0.0134mmol) was added as an oxidizing agent into the aqueous solution, and stirred acutely at RT until the color of solution changed from original orange to green. The green solution was detected by using UV-vis spectroscopy. Next, the equimolar L-sodium ascorbate solution (2.66mg, 0.0134mmol) was adopted as a reducing agent and added into the green solution. The vigorous stirring was then conducted at RT until the color of the solution change from green to yellow. Finally, the UV-vis spectrum of the reduced solution was recorded.

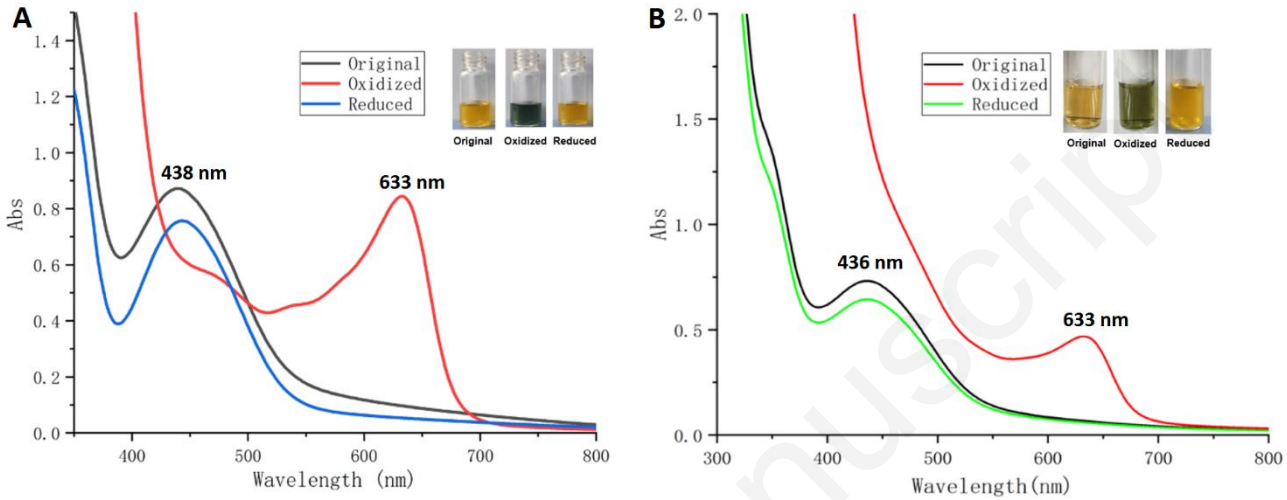

Figure S25 UV–vis. spectra of monomer **7** (A) and homopolymer **8a** (B) in water during an oxidation-reduction cycle.

6. Synthesis of the crosslinking agent 10

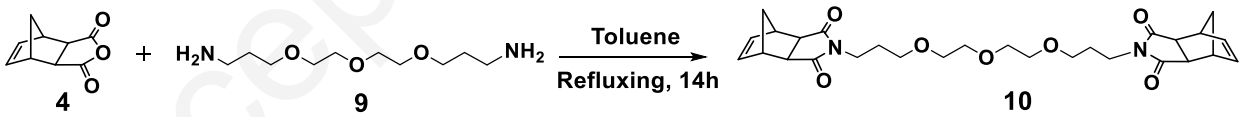

Scheme S1 The synthesis route of crosslinking agent **10**.

Cis-5-norbornene-*exo*-2,3-dicarboxylic anhydride (**4**, 5.0 g, 30 mmol, 1 equiv), Et_3N (3.1 g, 30 mmol, 1 equiv) and 4,7,10-trioxa-1,13-tridecanediamine (**9**, 3.3 g, 15 mmol, 0.5 equiv) were dissolved in toluene (50 mL) in a 250 mL round-bottomed flask. The obtained reaction mixture was stirred at 135 °C for 12 h under N_2 atmosphere. The solvent was then removed using a rotary evaporator, and the residue was purified by column chromatography with petroleum ether/ethyl acetate (5/1, v/v) as the eluent to provide the crosslinking agent **10** as colorless viscous liquid. Yield: 90%. ^{1}H NMR (400 MHz, $CDCl_3$, 25 °C, TMS), δ_{ppm}: 6.26 (t, *J* = 1.8 Hz, 2H, 2 × CH=CH), 3.52-3.61 (m, 12H, 3 × CH_2OCH_2), 3.43 (t, *J* = 6.2 Hz, 4H, 2 × $CONCH_2$), 3.23 (t, *J* = 1.3 Hz, 4H, 2 × =CH-C***H***), 2.64 (d, *J* = 0.6 Hz, 4H, 2 × CHCON), 1.81 (m, 4H, 2 × $OCNCH_2CH_2$), 1.48 (double broad, 2H, CH_2 of cyclopentane), 1.21 (double broad, 2H, CH_2 of cyclopentane). ^{13}C NMR (100 MHz, $CDCl_3$, 25 °C, TMS), δ_{ppm}: 178.1 (CON), 137.8

(CH=CH), 70.5 (OCH_2), 70.2 (OCH_2), 68.7 (OCH_2), 47.8 (CH_2-bridge), 45.1 (***C***HCON), 42.8(=CH***C***H), 36.2 (OCNC***H₂***CH_2), 27.9 ($OCNCH_2C$***H₂***).

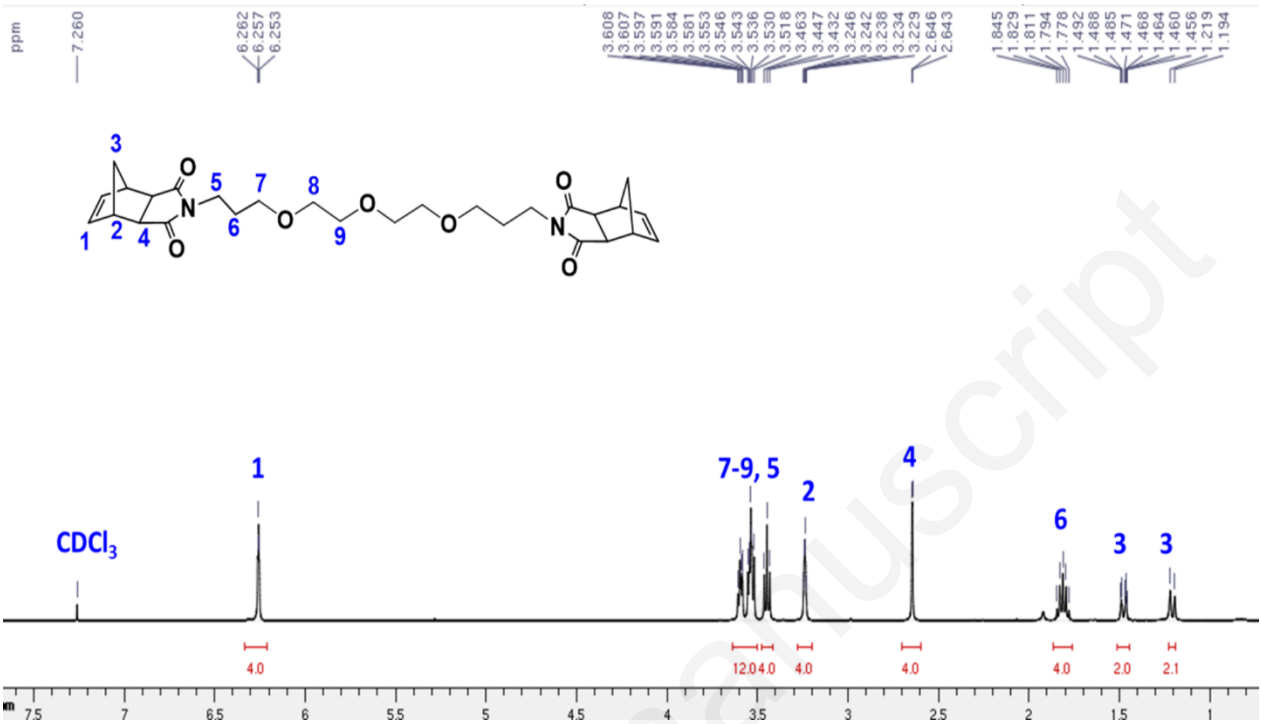

Figure S26 ^{1}H NMR spectrum of **10** in $CDCl_3$.

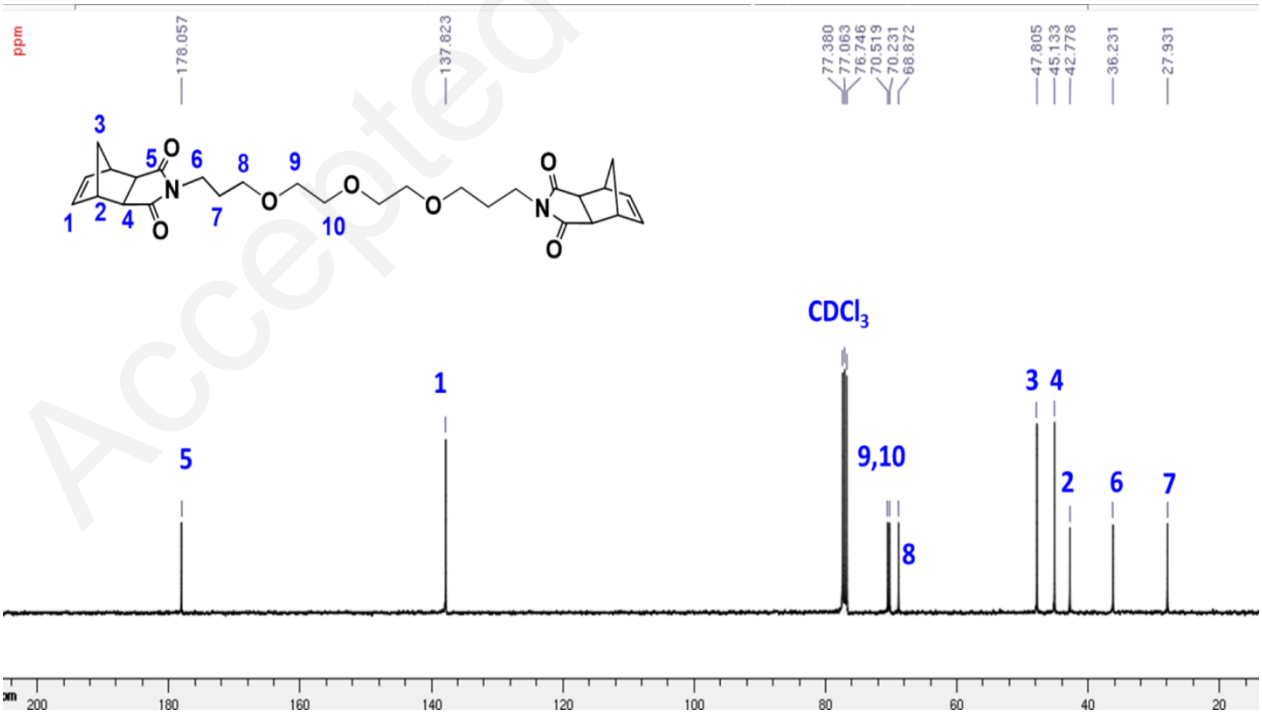

Figure S27 ^{13}C NMR spectrum of of **10** in $CDCl_3$.

7. Preparation and characterization of the Fc-containing hydrogels

Covalent cross-linking Fc-containing hydrogel (CC-Fc-HG):

Monomer **7** (200 mg, 0.268 mmol, 100 equiv), crosslinking agent **10** (54.88 mg, 0.1072 mmol, 40 equiv) and catalyst A (2.37 mg, 0.00268 mmol, 1 equiv) were dissolved in 3 mL of DMF in a small test tube. The obtained mixture was dramatically stirred for 30 min at RT under N_2 atmosphere, and the reaction solution then solidified to a gel. The formed gel was taken out, and added into a dialysis bag with molecular weight cut off (MWCO) of 3500 Da. The dialysis treatment was conducted against distilled water (1000 mL) at RT for 5 days, and, during this period, the dialysate was replaced by freshly distilled water every 12 h. Finally, the obtained hydrogel **Fc-HG** was freeze-dried in a vacuum freeze drier.

Supramolecular β-CD/Fc host-guest interaction based hydrogel S-Fc@β-CD-HG-1:

The saturated aqueous solution of β-CD was prepared by dissolving 18 g of β-CD in distilled water (1000 mL). The organo-gel was firstly prepared in DMF following the above procedure. The formed gel was taken out and added into a dialysis bag (the dialysis bag was treated in boiling water for half an hour in advance) with MWCO of 3500 Da. The dialysis treatment was conducted against the saturated aqueous solution of β-CD (1000 mL) at RT for 5 days and, during this period, the dialysate was replaced by the freshly saturated aqueous solution of β-CD every 12 h. The hydrogel was then subjected to dialysis in deionized water at RT for 5 days and during this period, the dialysate was replaced by freshly distilled water every 12 h to remove the free β-CD. Finally, the obtained hydrogel **S-Fc@β-CD-HG-1** was freeze-dried in a vacuum freeze drier.

Supramolecular β-CD/Fc host-guest interaction based hydrogel S-Fc@β-CD-HG-2:

Monomer **7** (200 mg, 0.268 mmol, 100 equiv) and β-CD (304.9 mg, 0.268 mmol, 100 equiv) were dissolved in 2 mL of DMF in a small test tube, and then stirred at RT for 48 h under N_2 atmosphere. After that, crosslinking agent 10 (54.88 mg, 0.1072 mmol, 40 equiv), catalyst A (2.37 mg, 0.00268 mmol, 1 equiv) and 3 mL of DMF were added into the test tube. The obtained mixture was further dramatically stirred at RT under N_2 atmosphere, and after 2 h of stirring, the formation of gel could be observed. The formed gel was taken out, and added into a dialysis bag with MWCO of 3500 Da. The dialysis treatment was conducted against distilled water (1000 mL) at RT for 5 days, and during this period, the dialysate was replaced by freshly distilled water every 12 h. Finally, the obtained hydrogel S-Fc@β-CD-HG-2 was freeze-dried in a vacuum freeze drier.

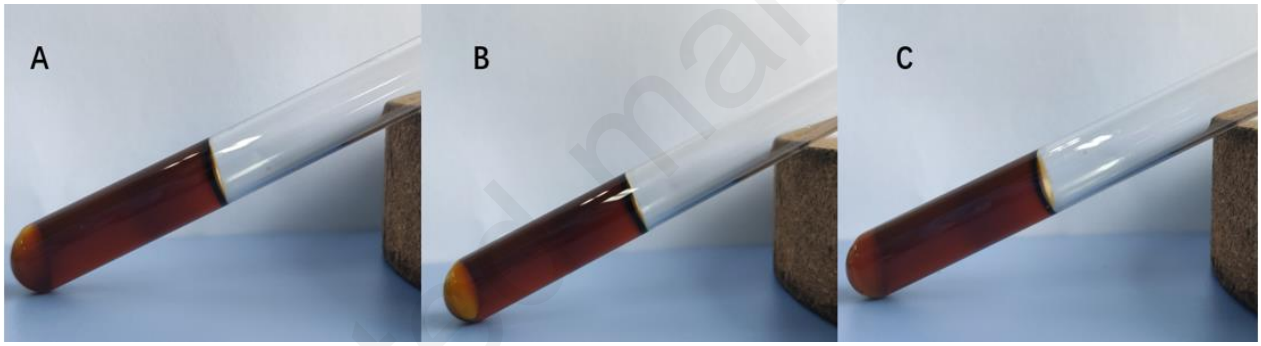

Figure S28 Photographs of gels **CC-Fc-HG** (A, B), and **S-Fc@β-CD-HG-2** (C) in DMF.

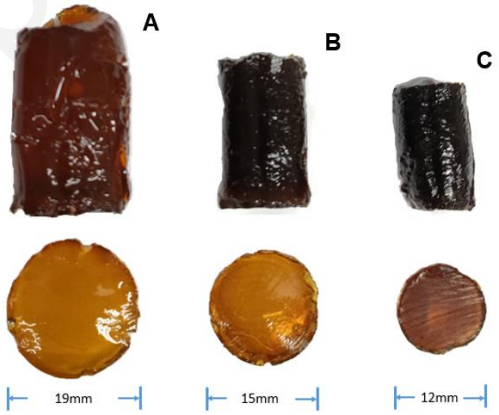

Figure S29 Photographs of swelling hydrogels (after dialysis in water) **CC-Fc-HG** (C), **S-Fc@β-CD-HG-1** (B) and **S-Fc@β-CD-HG-2** (A) and their cross sections with diameters.

7.1. Determination of water-absorbing property

One piece of the freeze-dried hydrogel (100 mg) was added into a big beaker, and 100 mL of deionized water was then poured into the beaker to immerse the hydrogel piece. Hereafter, the beaker was placed at room temperature (25 °C or so) for 120 h. At different intervals, the hydrogel piece was taken out, wiped by using the test paper to remove the water on its surface, and then weighed. After that, the hydrogel piece was replaced into the beaker containing deionized water. The water absorption rate (WAR) was calculated using the following formula.

$$WAR(\%) = \frac{W_t - W_0}{W_0} \times 100\%$$

W_t is the weight (mg) of swelling hydrogel piece at t h of soaking, and W_0 is the original weight (mg) of dried hydrogel piece. The water absorption curve was drawn by using the soaking time as the x-coordinate and WAR as the y-coordinate.

7.2. Redox-responsivity of the hydrogels

A hydrogel disc was immersed in 5 mL of hydrogen peroxide (H_2O_2, 35%) in a petri dish. The oxidation treatment was conducted for 1 h at RT. During this period, the color changed from the original orange to green. After that, the green hydrogel disc was taken out and wiped by using the test paper to remove the H_2O_2 solution on its surface. Then, the disc was put into a new petri dish containing 5 mL of glutathione (GSH) solution (50 mg/mL). The reduction treatment was conducted for 1 h at room temperature, too, and the color change was observed from green to orange.

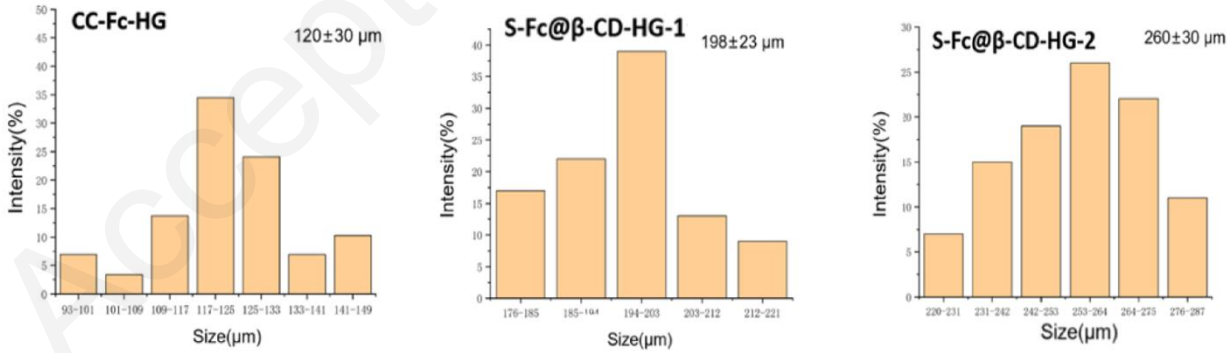

Figure S30 Pore sizes by SEM of the original **CC-Fc-HG**, **S-Fc@β-CD-HG-1** and **S-Fc@β-CD-HG-2**.

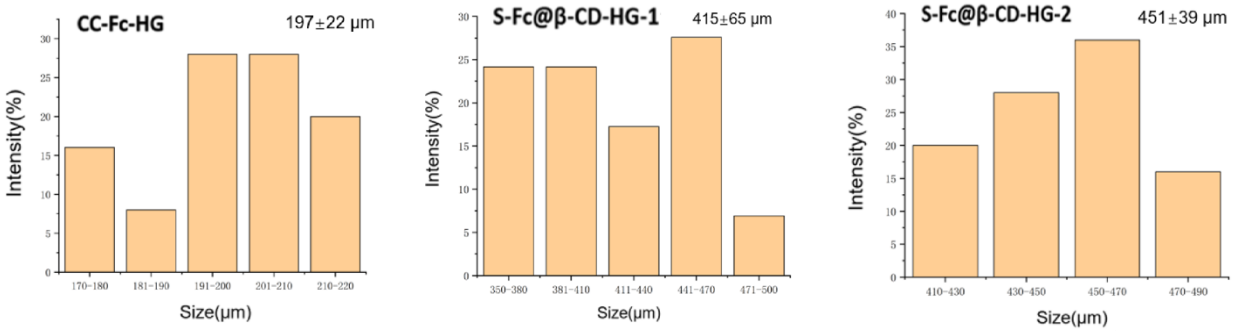

Figure S31 Pore sizes by SEM of the oxidized **CC-Fc-HG**, **S-Fc@β-CD-HG-1** and **S-Fc@β-CD-HG-2**.

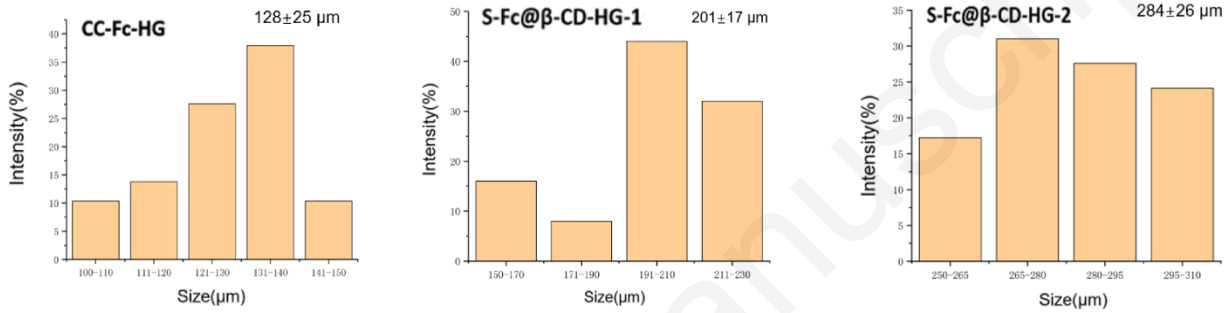

Figure S32 Pore sizes by SEM of the reduced **CC-Fc-HG**, **S-Fc@β-CD-HG-1** and **S-Fc@β-CD-HG-2**.